CLNS 90/1021
September 1990

Lectures given at the NATO Advanced Study Institute on Techniques and Concepts of High Energy Physics June 1990, St. Croix, U. S. Virgin Islands

INTRODUCTION TO THE PHYSICS OF PARTICLE ACCELERATORS

Robert Siemann

Newman Laboratory of Nuclear Studies
Cornell University
Ithaca, N. Y. 14853

INTRODUCTION

Progress in science is closely connected to the capabilities of instruments. Accelerators and detectors are the instruments of particle physics; these lectures are devoted to the former. Examples of relationship between accelerator science and particle physics are the discovery of the W and Z bosons which was a result of the development of stochastic cooling and the extensive studies of c- and b-quarks have been critically dependent on understanding and improvement of e^+e^- storage rings. In the future work on superconducting magnets could lead to the discovery of the t-quark and the Higgs.

In an accelerator charged particles move in electromagnetic fields. The motion can be classical or quantum mechanical, and the fields can be static or time dependent, externally applied or beam generated, and linear (proportional to displacement) or nonlinear. Combinations of all these possibilities occur and can be important. For example:
1. The SSC and LHC apertures are determined by classical motion in static, externally applied, nonlinear fields.
2. The luminosity limit of heavy quark factories depends in part on classical motion in time dependent, beam generated, nonlinear fields.
3. Quantum mechanical effects due to time dependent, beam generated fields at the collision point influence linear collider parameters strongly.

The usual approach is to understand the dominant contributions to the motion first and then treat other aspects as perturbations. This dominant motion is that of single particles undergoing classical motion in externally applied, linear fields. Both static and time dependent fields are important.

SINGLE PARTICLE MOTION

Figure 1 is a sketch of a linear accelerator consisting of accelerating RF cavities with quadrupole lenses interspersed. There is a fictitious *Ideal* particle that is on-axis and at the nominal energy (which increases linearly with s, the distance along the accelerator). Real particles can deviate from the *Ideal* by being off-axis and/or at other than the nominal energy. Concentrate on the energy motion first.

Energy Motion

The RF wave in the accelerating cavities can be thought of as propagating in the +s direction with phase velocity equal to c, the speed of light. At a fixed s the accelerating electric field is

1360790-008

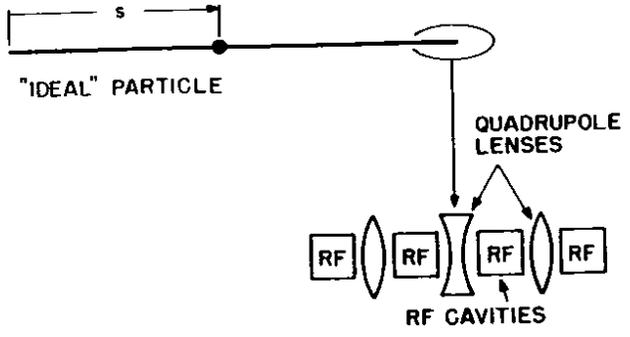

Fig. 1. A sketch of a linear accelerator.

$$E_{RF} = G \cos(\omega_{RF} t) \qquad (1)$$

where G is the accelerating gradient (with units of V/m) and ω_{RF} is the RF (angular) frequency. Consider a particle that passes at a time τ later than the *Ideal* which is at the crest of the wave (Figure 2a). Assuming the particle and the *Ideal* are relativistic, the equations of motion are

$$\frac{d\gamma}{ds} = \frac{e}{mc^2} G \cos(\omega_{RF}\tau) \quad \text{and} \quad \frac{d\tau}{ds} = 0 \qquad (2)$$

where e is the electric charge of the particle and γ is the energy of the particle in units of the rest energy mc^2. A bunch of such particles has a stable shape - particles at the head of the bunch remain there over the entire length of the accelerator, and there is a correlation between energy and τ - the fractional energy spread σ_γ/γ is proportional to σ_τ where σ_τ is the rms time spread of the bunch.

Figure 3 is a sketch of a storage ring. It consists of dipole magnets that bend particles in a circle, quadrupoles for focusing, and an RF cavity. Again, there is an *Ideal* particle that is on-axis and at the nominal energy, γ_0, which is constant for a storage ring. The *Ideal* is located at a different place on the RF wave because the nominal energy is constant (Figure 2b). The equations of motion of a particle passing through the RF cavity are given by eq. (2) with the argument of the cosine being $\omega_{RF}\tau + \pi/2$ instead of $\omega_{RF}\tau$. For one passage through the cavity

1360790-009

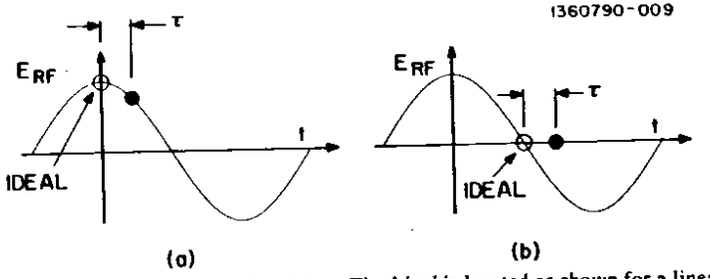

Fig. 2. The RF wave at a fixed position. The *Ideal* is located as shown for a linear accelerator (a) and a storage ring (b).

1360989-079

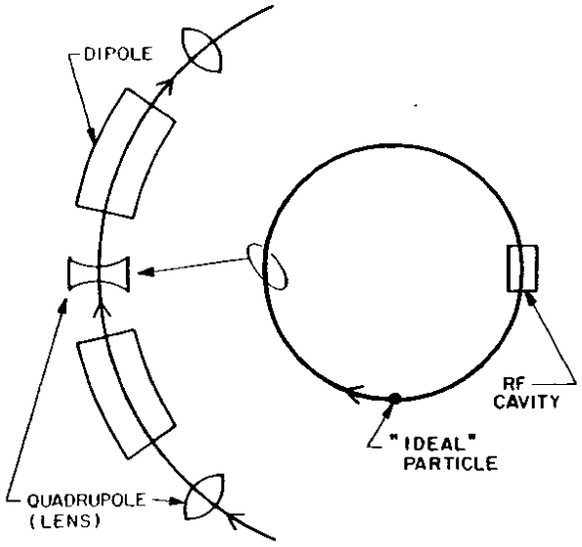

Fig. 3. A sketch of a storage ring.

$$\Delta\gamma \cong \frac{-eGL}{mc^2}\omega_{RF}\tau \quad \text{and} \quad \Delta\tau = 0 \qquad (3)$$

where L is the RF cavity length.

The particle is bent in a circle between passages through the RF cavity. Consider only the dipoles for a moment. In bending through an angle $d\theta$ the *Ideal* travels a distance $ds = Rd\theta$ where R is the bending radius of the *Ideal*, and a particle with energy γ travels $ds' = R(1 + (\gamma-\gamma_0)/\gamma_0)d\theta$. This particle takes a different amount of time to travel $d\theta$ because $ds' \neq ds$, and τ varies as $d\tau/ds = (\gamma-\gamma_0)/(c\gamma_0)$. The quadrupoles are important because they provide additional bending. When this is accounted for $d\tau/ds = \alpha(\gamma-\gamma_0)/(c\gamma_0)$ where α is called the momentum compaction and is in the range 0.001 to 0.05 depending on the quadrupole configuration. For a passage around the arc

$$\Delta\gamma = 0 \text{ and } \Delta\tau = \alpha T_0 \frac{\gamma-\gamma_0}{\gamma_0} \qquad (4)$$

where T_0 is the revolution period.

The motion described by eqs. (3) and (4) is an oscillation about the *Ideal*. This can be seen by looking at particles at different positions in the longitudinal phase space shown in Figure 4. This oscillation is called a synchrotron oscillation and corresponds to a particle interchanging energy and time displacements. The underlying principle was discovered by McMillan in 1945.[1] The frequency of oscillation can be determined by making the approximations $d\tau/dt \cong \Delta\tau/T_0$ and $d\gamma/dt \cong \Delta\gamma/T_0$ where $\Delta\tau$ and $\Delta\gamma$ come from eqs. (4) and (3), respectively. The resultant expressions can be combined to give

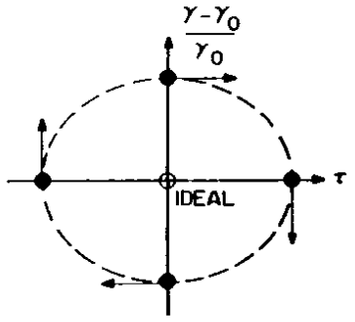

Fig. 4. Longitudinal phase space with four particular points shown. The arrows indicate the direction of motion given by eqs. (3) and (4). If these points are connected together, oscillatory motion results.

$$\frac{d^2\tau}{dt^2} = \frac{\alpha}{\gamma_0}\frac{d\gamma}{dt} = \frac{-eG\,L\alpha\omega_{RF}}{mc^2\gamma_0 T_0}\,\tau \quad . \tag{5}$$

This is the equation for simple harmonic motion with angular frequency, the synchrotron frequency,

$$\omega_s = \left(\frac{eG\,L\alpha\omega_{RF}}{mc^2\gamma_0 T_0}\right)^{1/2} \quad . \tag{6}$$

The "synchrotron tune" is the number of synchrotron oscillations per revolution. It is $Q_s = \omega_s T_0/2\pi$.

Particles oscillate about the position of the *Ideal* which is the point where the RF voltage is zero and has a negative slope. The RF phase advances by an integer multiple of 2π each time the *Ideal* makes a turn - a passage around the ring. This is the only way it can have the same position on successive turns. This means that the orbital period must be a multiple of the RF period, $T_0 = h\,(2\pi/\omega_{RF})$ where h is an integer called the harmonic number. The RF frequency, not the dipole field strength, determines the accelerator circumference! This simple argument has another consequence. There are h positions equally spaced around the ring where the *Ideal* could be located. Therefore, h is the number of bunches the ring can hold.

The analysis above that led to eqs. (4) and (5) assumed relativistic particles. There are two effects that are important for non-relativistic particles traveling in a circle between passages through the RF cavity. If the energy is greater than that of the *Ideal* the path length is longer and the velocity is greater. The latter is more important below the "transition energy". Non-relativistic particles undergo synchrotron oscillations also; the difference is that the position of stable equilibrium is located at the point where the RF voltage is zero but has a positive slope.

Transverse (Betatron) Motion

Particles have transverse displacements and angles with respect to the trajectory of the *Ideal*. The quadrupole magnets provide the focusing needed to contain the beam.

In a current free region the magnetic field is the gradient of a scalar potential, $\mathbf{B} = -\nabla\phi$. For the quadrupole magnet shown in Figure 5, $\phi = gxy$; g is called the quadrupole gradient and has units of T/m. The equation of motion, $d\mathbf{p}/dt = e\mathbf{v} \times \mathbf{B}$, can be broken-up into x and y components. For the x component $dp_x/dt = -ecB_y = ecgx$ becomes

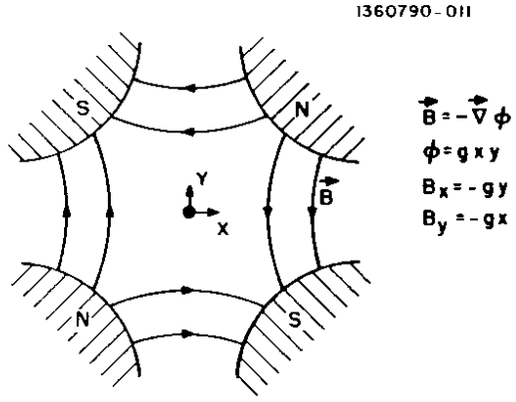

Fig. 5. A quadrupole magnet.

$$\frac{d^2x}{ds^2} = \frac{eg}{\gamma mc}\,x \tag{7}$$

when p_x is approximated as $p_x \cong \gamma mc\,dx/ds$. This is the equation for simple harmonic motion if $eg/\gamma mc < 0$, and the x motion is bounded in this case. When $eg/\gamma mc > 0$ there is exponential growth and unbounded motion.

For the y component the equation of motion is

$$\frac{d^2y}{ds^2} = -\frac{eg}{\gamma mc}\,y \quad . \tag{8}$$

If the motion is bounded in x, it grows exponentially in y and vice versa. This is a consequence of the magnetic field being derived from a scalar potential which in turn is a consequence of the beam traveling in a current free region.

A single quadrupole can focus in only one transverse dimension at a time, and to have focusing in both x and y multiple quadrupoles arranged as a compound optical system are needed. A simplified arrangement is shown in Figure 6. The fact that such compound systems can be constructed with bounded motion in both x and y is the principle of "strong focusing".[2] The equation of motion in one transverse dimension is

$$\frac{d^2x}{ds^2} = \frac{eg(s)}{\gamma mc}\,x = k(s)\,x \tag{9}$$

where $k(s) < 0$ in focusing quadrupoles, $k(s) = 0$ in field free regions, and $k(s) > 0$ in defocusing quadrupoles. The motion looks like simple harmonic motion, but the variation of k with s makes it more complicated. However, it is natural to look for an oscillatory solution of the form

$$x = A\,w(s)\,e^{i\psi(s)} \tag{10}$$

Such a solution exists if w(s) and $\psi(s)$ satisfy[2]

$$\frac{d^2w}{ds^2} + k(s)\,w - \frac{1}{w^3} = 0 \tag{11}$$

and

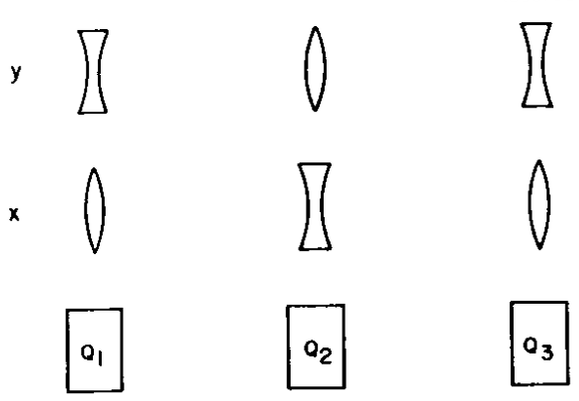

Fig. 6. A sketch showing alternating gradient focusing - an array of alternating focusing and defocusing quadrupoles. This arrangement is used in the simplified *SSC* discussed below. In that example the quadrupoles are 5.05 m long, there is 180 m from the center of Q_1 to the center of Q_3, and each quadrupole has |g| = 211 T/m.

$$\frac{d\psi}{ds} = \frac{1}{w^2} \quad . \tag{12}$$

Equation (11) is called Hill's equation.

There are a number of important comments that can be based on eqs. (11) and (12).
1. w(s) depends on the "lattice" - the configuration of quadrupoles - through the second term on the left-hand-side of eq. (11).
2. However, w(s) is not uniquely determined by the lattice; eq. (11) is a second order differential equation and two constants of integration are needed for a unique solution.
3. w(s) has an absolute scale; i.e. if $w_1(s)$ is a solution, $2\,w_1(s)$ is not.
4. The phase advance, dψ/ds, is not constant but is given by eq. (12).

Accelerator physicists often call transverse motion "betatron motion" and talk about the "β-function" of a storage ring, a beam transport, or a linear accelerator. It is related to w(s) by $\beta(s) = \{w(s)\}^2$. In terms of β eq. (12) is

$$\frac{d\psi}{ds} = \frac{1}{\beta(s)} \quad , \tag{13}$$

and the motion of a particle is

$$x = A\,\{\beta(s)\}^{1/2} e^{i\psi(s)} \quad . \tag{14}$$

Some initial conditions must be specified to determine β for a beam transport or linear accelerators, but there is a unique definition for a circular accelerator. The lattice of a circular accelerator is periodic, k(s + C) = k(s) where C is the circumference, and the β-function of a circular accelerator is the periodic solution to Hill's equation, β(s + C) = β(s).

Storage ring lattices usually consist of arcs where the β-functions are repetitious and interaction regions where the beams are focused for collisions. As a first example consider a simplified *SSC* without interaction regions and consisting of 500 cells one of which is illustrated in Figure 6. The β-functions are shown in Figure 7; they are large where the quadrupoles are focusing and small where they are defocusing. The β-function is periodic with period C, but the motion given by eq. (14) is not. Figure 8a shows the trajectory of a particle on two successive turns, and Figure 8b shows the trajectories on 100 successive turns.

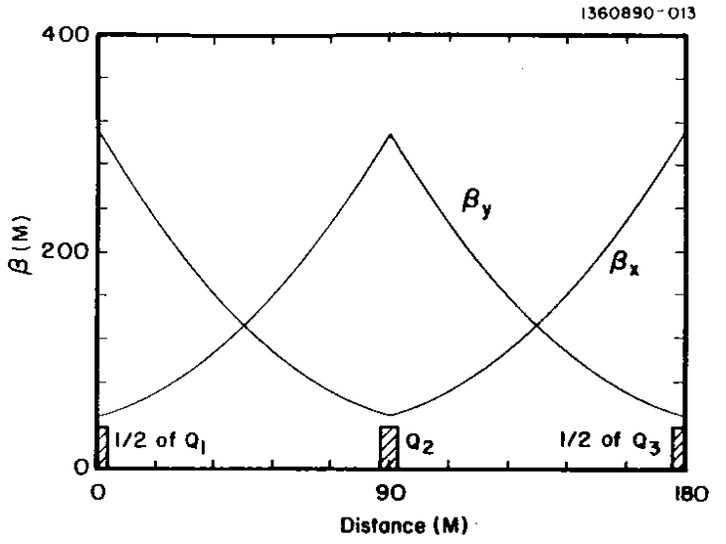

Fig. 7. The β-functions for one cell of the simplified *SSC* lattice.

Figure 9 shows the phases; they advance rapidly when β is small and slowly when β is large. The number of betatron oscillations per revolution is

$$Q_\beta = \frac{1}{2\pi} \oint_0^C \frac{ds}{\beta(s)} \quad ; \tag{15}$$

Q_β is called the betatron tune. For the simplified *SSC* Q_β = 127.80.

The β-function measures the sensitivity to errors in addition to giving the beam envelope and the rate of phase advance. If there is a gradient error δg in a quadrupole of length L located at a position s_e, there will be a change in tune[2]

$$\delta Q_\beta = -\frac{1}{4\pi}\beta(s_e)\frac{e\,\delta g L}{\gamma m c} \quad . \tag{16}$$

Large β leads to a large change of tune and high sensitivity to field errors.

Collider interaction regions are designed to have low β's for two reasons. First, the luminosity is given by

$$L = \frac{N^2 f_c}{4\pi\sigma_x\sigma_y} \tag{17}$$

where N is the number of particles per bunch, f_c is the collision frequency and $4\pi\sigma_x\sigma_y$ is the effective collision area. Since σ_x and σ_y are proportional to $\sqrt{\beta_x}$ and $\sqrt{\beta_y}$, respectively, low β reduces the effective area and increases the luminosity. Second, particles in one beam interact with the electromagnetic fields produced by the opposing beam. These fields are roughly equivalent to an error, and small β reduces the sensitivity to this error. This is discussed in more detail in the section about beam-beam effects.

The β-function at the collision point is usually denoted by β^*. At a distance S from the collision point before the first quadrupole is encountered $\beta(S) = \beta^* + S^2/\beta^*$. (This can be shown from eq. (11) using the fact that β is a minimum at the collision point and k(s) = 0

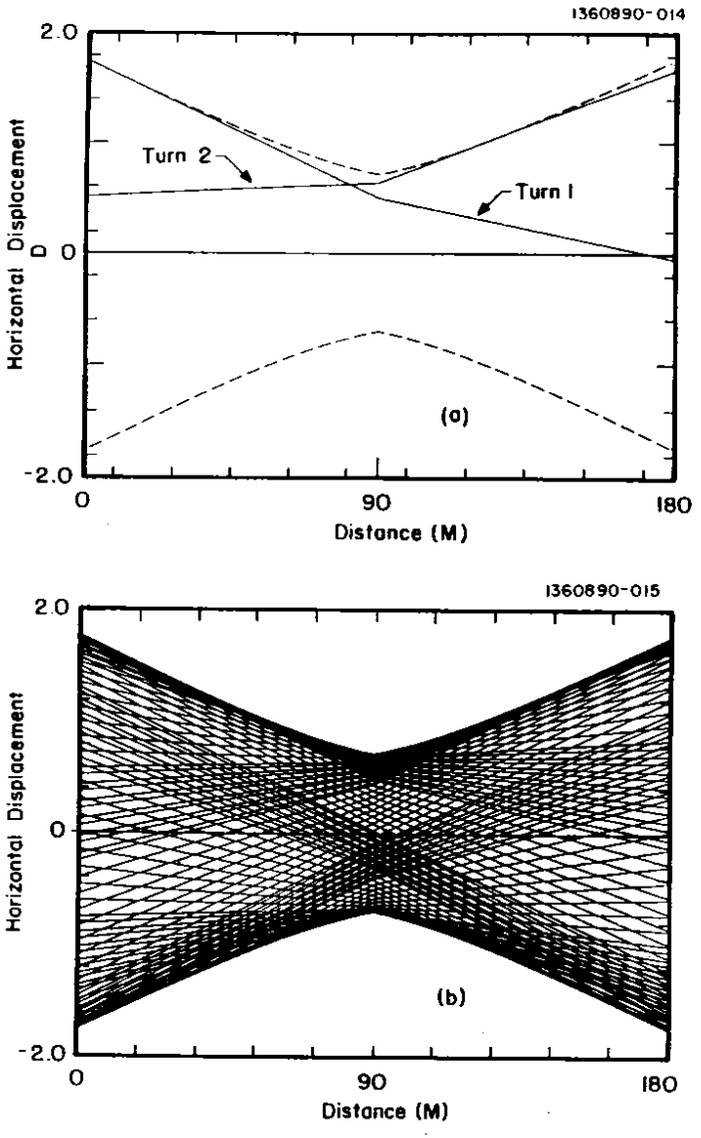

Fig. 8. Horizontal (x) trajectories on successive turns. The dashed lines are proportional to $\pm\sqrt{\beta_x}$. (a) shows two turns and (b) shows 100 turns.

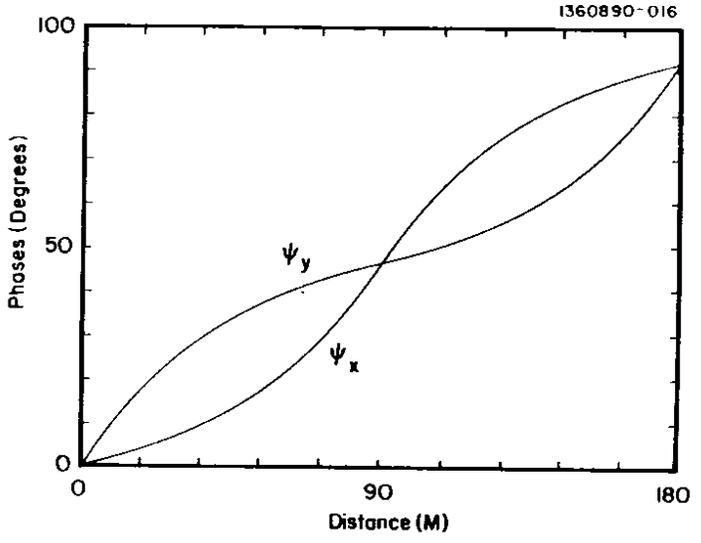

Fig. 9. The betatron phases for the simplified *SSC* lattice.

in the region before the first quadrupole.) With a small β_x^* the beam size increases rapidly as it leaves the collision point. Figure 10 shows a low β^* interaction region for the SSC.[5] There are three strong quadrupoles arranged in an alternating gradient configuration called a quadrupole triplet that gives $\beta^* = 0.5$ m in both dimensions. The first quadrupole begins 20 m from the collision point; $\beta \sim 800$ m at that point. This quadrupole can focus in only one dimension, and the beam is defocused in the other. The β-function in that dimension grows rapidly. It reaches a peak value of about 8000 m before being turned around by the next quadrupole in the triplet. The beam size has grown by about a factor of 125, and because of the large β's in these quadrupoles, their field quality in important. The combination of demands on the interaction region quadrupoles - high gradient, large aperture and good field quality - make these quadrupoles one of the technological marvels of modern colliders. After the triplet the lattice is arranged to restore the smooth β-functions such as shown in Figure 7.

Emittances

The β-function gives the variation of the beam size with position s, but it doesn't give the actual beam size. For that one needs to know the typical amplitude of oscillation, A, in eq. (14). The "transverse emittance" of a beam, ϵ, is defined as

$$< A^2 > \equiv 2\epsilon \quad . \tag{18}$$

(A word of caution is necessary; different laboratories use different proportionality constants between ϵ and $< A^2 >$.) The rms beam size at position s is

$$\sigma_z(s) = [\beta_z(s)\epsilon]^{1/2} \tag{19}$$

where z is either x or y. A longitudinal emittance associated with the synchrotron oscillations can be defined in the same manner. The discussion below is restricted to one transverse dimension, but it holds equally well for the other transverse dimension, and a similar one holds for the longitudinal emittance.

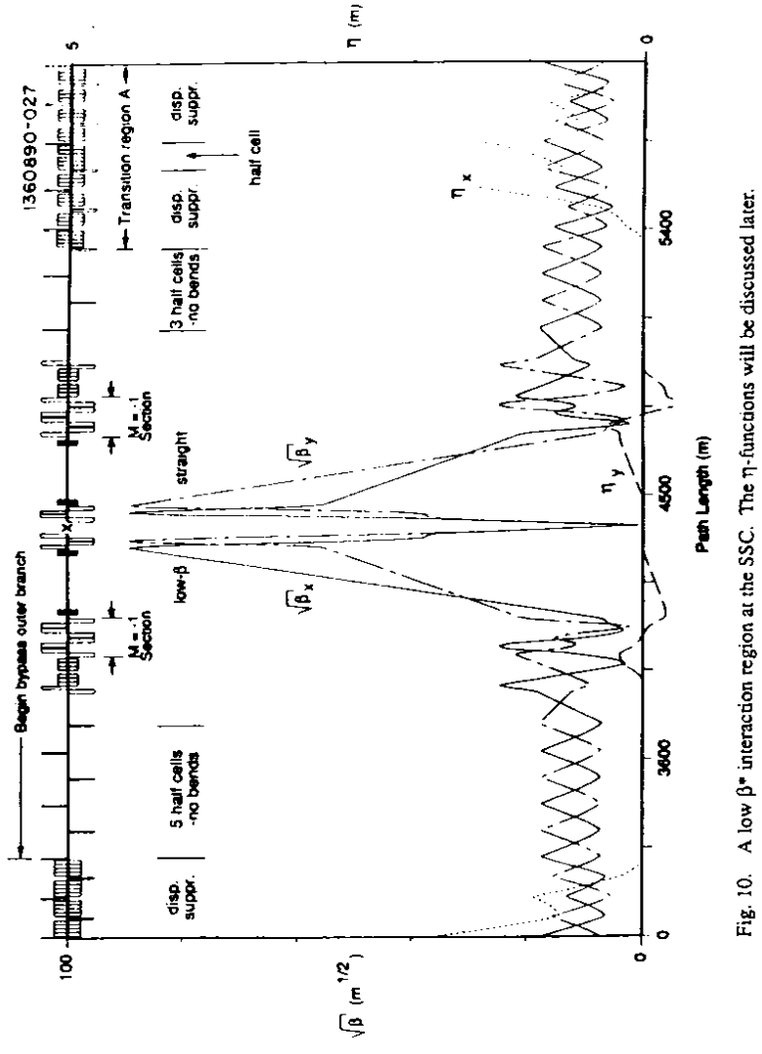

Fig. 10. A low β* interaction region at the SSC. The η-functions will be discussed later.

The amplitude of a particle can be written in terms of its position and angle

$$A^2 = \frac{x^2}{\beta} + \beta\left(x' - \frac{\beta'}{2\beta}x\right)^2 \qquad (20)$$

where $\beta' = d\beta/ds$. Equation (20) is the equation of an ellipse in *transverse phase space*, a space with axes x and x'. The amplitude A is independent of position, s, even though x, x', β and β' all depend on position; i.e. a particle with amplitude A remains on this ellipse as it moves around the accelerator. The area of the ellipse given by eq. (20) is πA^2, and the emittance measures the phase space area occupied by the beam.

Liouville's Theorem[4] puts constraints on the emittance; it says that the area occupied in a phase space with axes x and $\gamma\beta_v x'$ (the canonical momentum of x) cannot change in time; β_v is the usual relativistic velocity, $\beta_v = v/c$. Therefore, $\gamma\beta_v\varepsilon$ is constant as a beam is accelerated, transported down a beam line, etc. whenever Liouville's Theorem is valid. It is in proton accelerators and linear electron accelerators, but it isn't in electron storage rings and anti-proton sources. For specificity consider a proton accelerator first. The beam originates in an ion source, and the emittance is determined by the properties of ion sources. The beam is accelerated first in a linac and then in a number of synchrotrons before reaching collision energy. During all these process the emittance shrinks as $1/\gamma\beta_v$. Except for this decrease with energy the beam size at collision energies is determined by the physics of ion sources! It isn't surprising that particle sources are an active area of research.

The above discussion is not complete because it is impractical. A beam may develop a complicated, filament-like structure enclosing empty regions of phase space as it is accelerated. Theoretically, these filaments can be untangled, but that is impractical, and the effective phase space area of a beam tends to increase. The emittance behavior implied by Liouville's Theorem is the best possible, and in most cases emittances increase from the minimum given by Liouville's Theorem.

Liouville's Theorem isn't valid if there is damping or energy loss. There is energy loss in the form of synchrotron radiation in electron storage rings and anti-proton sources have stochastic cooling systems for damping. Therefore, $\gamma\beta_v\varepsilon$ is not constant, but it can be reduced. The possibilities depend on the physics and technology of the energy loss and damping mechanisms. These play the same role as the physics and technology of ion sources do for the proton accelerator discussed above.[5] This is too complex a subject for these notes, and it will have to suffice to say that within limits these accelerators can be designed to give a desired emittance.

WAKEFIELDS AND THEIR EFFECTS

The discussion has concentrated on single particles so far. Many interesting phenomena and performance limits come from interactions between particles. This section deals with one class of these interactions - beam current limits due to beam generated electromagnetic fields.

A beam passing a change in vacuum chamber profile radiates electromagnetic fields that propagate down the beam pipe in waveguide modes and, if a resonant structure is involved, excite normal modes. This is illustrated graphically in Figure 11.[6] At t = 0 the beam is entering the cavity, and the electric field is predominantly the space charge field of the beam. As time passes fields penetrate into the cavity, and cavity modes are excited. When the beam leaves at t = 2.0 nsec, it has lost energy to electromagnetic fields in the cavity. These beam induced fields, called wakefields, have many consequences:

1. The beam losses energy. This energy must be replaced by the RF system, and it can cause localized heating and damage to elements of the vacuum chamber.
2. Energy can be transferred from the head to the tail of a bunch.
3. The head of a bunch can deflect particles in the tail of the bunch.
4. Energy and deflections can be transferred between bunches if there are normal modes with large enough quality factors.

The last three can lead to emittance growth and instabilities.

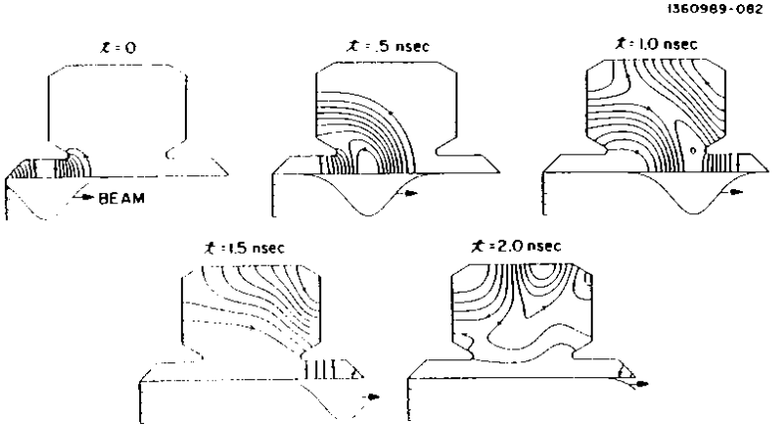

Fig. 11. The electric field lines produced by a Gaussian bunch passing through a LEP RF cavity.[6]

Wakefields

Consider the situation shown in Figure 12. Two ultrarelativistic particles Q and q are travelling in the z direction through a rotationally symmetric structure; Q has unit charge. The particles are a distance ct_0 apart; q trails Q when $t_0 > 0$. The particle positions with respect to the symmetry axis are given by vectors $\vec{R}_T$ and $\vec{r}_T$; ϕ is the angle between $\vec{R}_T$ and $\vec{r}_T$.

First, let Q travel on-axis, $\vec{R}_T = 0$. The "longitudinal wake potential" is the beam induced voltage seen by q

$$V_{\delta 0}(t_0) = \int_{-\infty}^{\infty} dz \int_{-\infty}^{\infty} dt' E_z(z,t') \delta(t' - (t_0 + z/c)) \quad . \qquad (21)$$

The quantity E_z is the longitudinal component of the electric field produced by Q. The wake potential $V_{\delta 0}$ has some simple properties illustrated by Figure 13. First, it is causal; $V_{\delta 0} = 0$ for $t_0 < 0$. Second, for positive t_0 as $t_0 \to 0$ $V_{\delta 0}$ must be negative because Q loses energy into the structure. At larger values of t_0 the wake potential depends on the structure geometry.

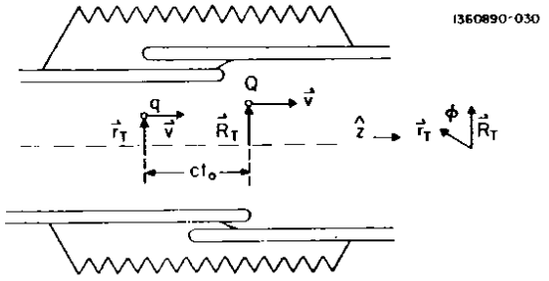

Fig. 12. Definition of the variables used to describe wakefields. The structure is assumed to be rotationally symmetric about the z-axis.

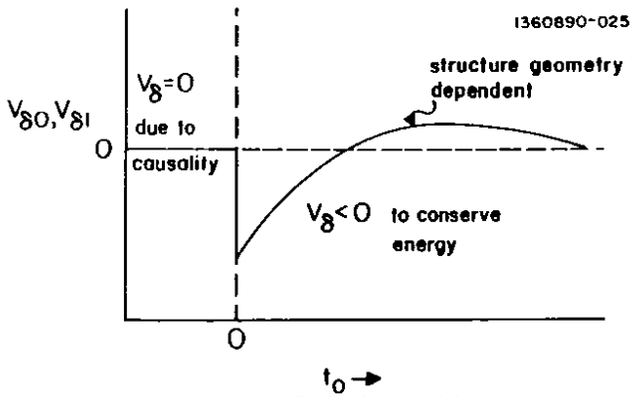

Fig. 13. Time dependence of the longitudinal wake potential.

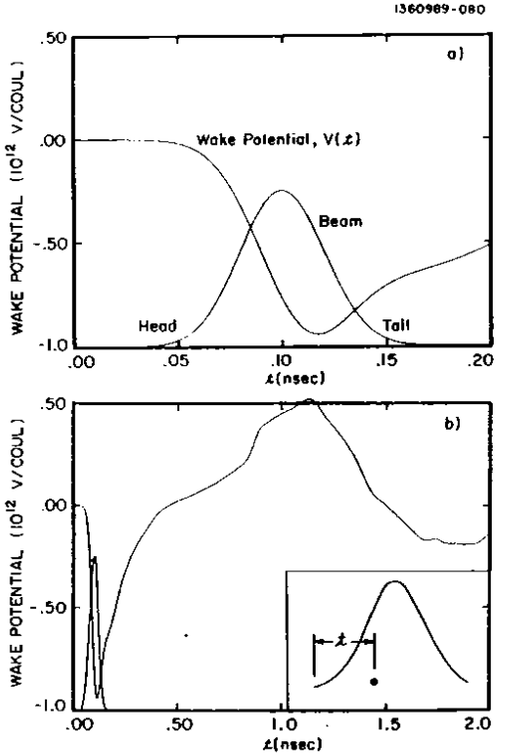

Fig. 14. The wake potential for a 6 mm long, 1 C bunch traveling through a CESR cavity shown on two different time scales. The inset defines the time t.

The wake potential for a bunch is given by the convolution of $V_{\delta 0}$ with the bunch charge density. It is proportional to N, the number of particles in the bunch, and depends on the rms bunch length and the structure geometry. A wake potential for a CESR RF cavity is plotted in Figure 14. Several of the consequences of beam induced fields mentioned above can be seen in this figure. First, the beam loses energy as is expected from a comparison of the electromagnetic field energies at t = 0 and t = 2 nsec in Figure 11. The energy loss is

$$\text{Energy change} = \int_{-\infty}^{\infty} dt\, I(t) V(t) < 0 \qquad (22)$$

where I(t) is the bunch current. The wake potential and I(t) are each proportional to N, so the energy loss is proportional to N^2. This "higher order mode" power is an important design consideration in heavy quark factories.[7] Second, Figure 14a shows that V(t) varies along the bunch; the wake potential is different at the head and tail. This introduces additional τ dependence into eq. (3) that can lead to the single bunch instabilities. Figure 14b shows that the wake potential can be positive at longer times, and a particle passing through the cavity at those times gains energy. Therefore, it is possible to transfer energy between bunches; this leads to coupled bunch instabilities.

If Q is not on-axis[8]

$$V_\delta(t_0) = \int_{-\infty}^{\infty} dz \int_{-\infty}^{\infty} dt'\, E_z(z,t')\,\delta(t' - (t_0 + z/c)) \qquad (23)$$

$$\cong V_{\delta 0}(t_0) + r_T R_\Gamma\, V_{\delta 1}(t_0)\cos\phi \ .$$

The new term comes from modes that have $E_z = 0$ on-axis and are excited by Q being off-axis. The arguments about the qualitative behavior of $V_{\delta 0}$ hold for $V_{\delta 1}$, so it has the general shape shown in Figure 13. When $V_{\delta 1} \neq 0$, $\partial E_z/\partial r \neq 0$ and it follows from Maxwell's equations that E and B have radial and azimuthal components that cause deflections. The deflection produced by Q is the $R^\rightarrow_T$ direction, and the magnitude, the "transverse wake potential",is

$$W_\delta(t_0) = \frac{1}{R_T} \int_{-\infty}^{\infty} dz \int_{-\infty}^{\infty} dt' \,(E(z,t') + v \times B(z,t'))_T \,\delta(t' - (t_0 + z/c)) \qquad (24)$$

where E and B are the fields produced by Q and the subscript T indicates the component in the $R^\rightarrow_T$ direction. The wake potentials $V_{\delta 1}$ and W_δ are not independent. They are related by the Panofsky-Wentzel Theorem[9]

$$W_\delta(t_0) = -\int_{-\infty}^{t_0} dt\ V_{\delta 1}(t) \ . \qquad (25)$$

Given the form of $V_{\delta 1}$ in Figure 13 and the Panofsky-Wentzel Theorem, the transverse wake potential is shown in Figure 15. For small t_0 q is displaced in the same direction as Q.

Impedances. Beam stability problems are often solved in the frequency domain. There one uses impedances rather than wake potentials. The longitudinal and transverse impedances, Z_L and Z_T, are related to the wake potentials by

$$Z_L(\omega) = -\int_{-\infty}^{\infty} dt\, V_{\delta 0}(t) e^{-i\omega t} \text{ and } Z_T(\omega) = i\int_{-\infty}^{\infty} dt\, W_\delta(t) e^{-i\omega t} \ . \qquad (26)$$

Emittance Growth in Linear Colliders

This is the first example of the effects of wakefields. It is discussed with the simplifying assumption that there are only two particles in the beam. Such two-particle models are valuable for understanding the underlying physics. In addition, they can be generalized to include more particles. This is usually the way computer simulations of beam stability are performed.

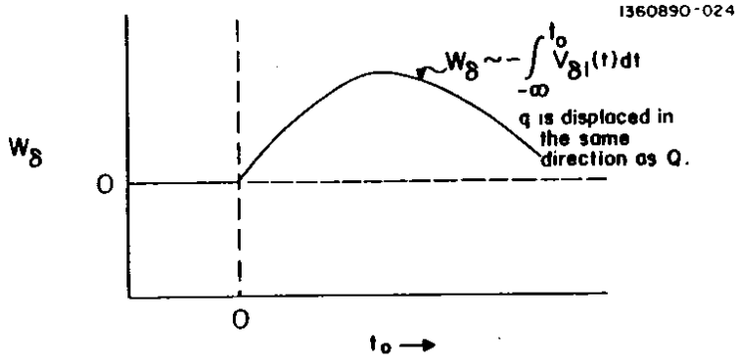

Fig. 15. Time dependence of the transverse wake potential.

If a particle is injected off-axis, the quadrupoles focus it and produce an oscillation about the axis. If a second particle, the *tail*, is injected following the first, the *head*, it experiences the wakefields produced by the *head*. For realistic bunch lengths the *tail* is in the short-time region of the transverse wake potential, and it is deflected in the direction of the *head*. Therefore, the *tail* is always deflected away from the axis by the *head*; see Figure 16. Its amplitude of oscillation grows thereby increasing the effective emittance of the beam. Figure 17a shows the results of a multiparticle simulation of the SLC with a 30 μm injection error.[10] Particles in the tail have experienced large deflections and can lower the luminosity and cause backgrounds while those at the head of the beam are near the axis.

Possible ways to control this emittance growth include removing misalignments and injection errors to the extent feasible, using strong quadrupoles to maximize focusing, choosing an accelerator with small wakefields, and using Balakin, Novokhatsky, and Smirnov (BNS) damping.[11] Concentrate on the last two of these. The bunch length, $c\sigma_\tau$, should be much less than the wavelength of the accelerating RF to keep the energy spread small. If $\sigma_\tau \omega_{RF}$ and the proportions of the accelerator are held fixed as ω_{RF} is changed, the transverse wake potential at the tail varies as ω_{RF}^2.[12] This argues for low frequencies and long wavelengths. On the other hand, the efficiency for transferring energy from the accelerating fields to the beam depends on ω_{RF} as ω_{RF},[12] and there is a trade-off between reducing wakefields and efficient operation. Frequencies that are currently favored by linear collider designers are in the 10 GHz to 30 GHz range. Those are to be compared with the SLAC frequency of 2856 MHz. The need for good operating efficiency has driven people to higher frequencies, and BNS damping is critical for controlling emittance growth.

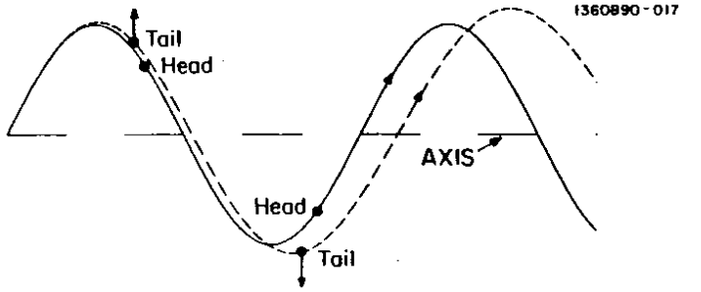

Fig. 16. The *head* is injected off-axis, and the quadrupoles produce an oscillation. The *tail* is always deflected in the direction of the *head* as indicated by the arrows.

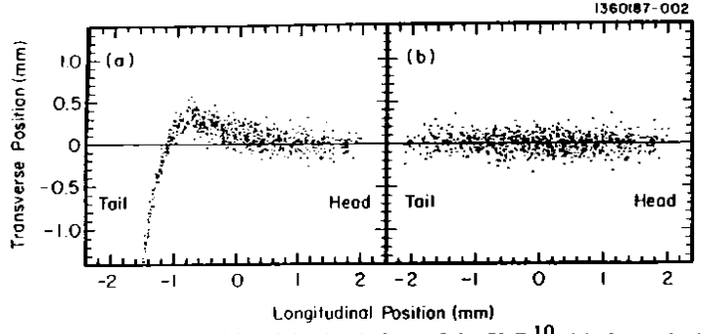

Fig. 17. The results of multiparticle simulations of the SLC.[10] (a) shows the large deflection of particles in the tail due to transverse wakefields. (b) shows the same situation when BNS damping has been applied.

BNS damping is analogous to an oscillator with an external drive. The driven response is greatest when the drive frequency equals the natural frequency, and there are beats between the driven response and oscillations (at the natural frequency) caused by non-zero initial conditions. In the linear collider the *head* drives the *tail*, and the emittance growth shown in Figure 17a can be reduced if $\omega_{head} \neq \omega_{tail}$, i.e. $\omega_{drive} \neq \omega_{nat.}$. BNS damping is produced at the SLC by making the energies of the head and tail different. That gives the quadrupoles different focusing strengths (eq. (7)) and the desired frequency inequality results. Figure 17b shows the power of BNS damping in the SLC. RF quadrupoles are being considered as an alternative approach to get different focusing at the head and tail.[13]

Instabilities in Circular Accelerators

There are a number of instabilities caused by wakefields in circular accelerators. The next two subsections are examples of them. They are chosen to illustrate the nature of instabilities and the interplay between various aspects of accelerator physics discussed to this point. Simple one and two particle models are used.

The Fast Head-Tail Instability. This important instability was discovered and interpreted at PETRA.[14] It affected the performances of both PETRA and PEP. In addition, the single bunch current in LEP is expected to be limited to about 0.75 mA by the fast head-tail instability, and, because of this, luminosity upgrades of LEP are concentrating on storing more bunches rather than increasing the single bunch current.

Consider two particles in a single bunch in a circular accelerator. The *head* produces a transverse wakefield that acts on the *tail*. The difference from the linear accelerator is that the *head* and *tail* interchange due to synchrotron oscillations (see Figure 18). This introduces new physics. As a simplification take the transverse wake potential to be $W(t_0) = W\Theta(t_0)$ where Θ is a step function.[15] Particle 1 is the *head*, and particle 2 is the *tail* for the first half of the synchrotron oscillation period. The *head* moves in simple harmonic motion

$$\frac{d^2y_1}{dt^2} + \omega_\beta^2 y_1 = 0 \qquad (27)$$

where the betatron motion has been approximated as smooth. The *tail* is driven by the *head*. Its equation of motion is

$$\frac{d^2y_2}{dt^2} + \omega_\beta^2 y_2 = \frac{N e^2 W}{\gamma m} y_1 \qquad (28)$$

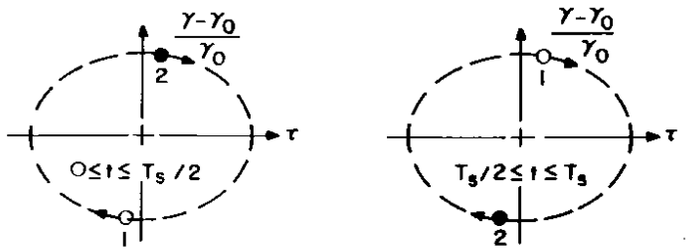

Fig. 18. The *head* and *tail* interchange every one-half synchrotron oscillation period, T_s.

where Ne is the charge of the *head*. Particle 2 is the *head* for the second half of the period, and the equations of motion are given by eqs. (27) and (28) with the indices interchanged, $1 \leftrightarrow 2$. Look for solutions of the form $y = Y(t)\exp(i\omega_\beta t)$ where $dY/dt << Y\omega_\beta$. Substituting into eqs. (27) and (28) Y_1 and Y_2 change by the following amounts during the first half period

$$\Delta Y_1 = 0 \text{ and } \Delta Y_2 = -\frac{i W N e^2 T_s}{4\omega_\beta \gamma m} Y_1 = \Xi Y_1 \qquad (29)$$

where T_s is the synchrotron oscillation period and this equation defines Ξ. The solution for a complete synchrotron oscillation period can be written in matrix form

$$\begin{pmatrix} Y_1 \\ Y_2 \end{pmatrix}_{T_s} = \begin{pmatrix} 1 & \Xi \\ 0 & 1 \end{pmatrix}\begin{pmatrix} 1 & 0 \\ \Xi & 1 \end{pmatrix}\begin{pmatrix} Y_1 \\ Y_2 \end{pmatrix}_0 = M\begin{pmatrix} Y_1 \\ Y_2 \end{pmatrix}_0 . \qquad (30)$$

For n synchrotron oscillations

$$\begin{pmatrix} Y_1 \\ Y_2 \end{pmatrix}_{nT_s} = M^n\begin{pmatrix} Y_1 \\ Y_2 \end{pmatrix}_0 . \qquad (31)$$

The motion is stable if all elements of M^n remain bounded as $n \to \infty$. Stability can be determined by looking at the eigenvalues of M. They are $\exp(\pm i\mu)$ where[2]

$$\cos\ \mu = \tfrac{1}{2}\times \mathrm{Tr}(M) = \tfrac{1}{2}\left(2 - \left(\frac{W N e^2 T_s}{4\omega_\beta \gamma m}\right)^2\right) . \qquad (32)$$

The motion is a stable oscillation as long as μ is real, i.e. $|\cos\mu| \le 1$. This gives the condition for stability

$$N \le \frac{8\omega_\beta \gamma m}{W e^2 T_s} . \qquad (33)$$

Equation (33) gives the instability threshold. Below that value this two particle system is stable. The amplitudes Y_1 and Y_2 oscillate but do not grow. Synchrotron motion has stabilized the beam and removed the potentially harmful effects of wakefields. This is in contrast to linear accelerators where there is no threshold for emittance growth. Above the threshold the amplitudes grow exponentially. The beam is unstable and doesn't fit into the vacuum chamber after a short amount of time.

Better calculations can be performed using realistic wakefields and many particles. These calculations verify the parametric dependences of eq. (33). Figure 19 shows results when the current is just above threshold. These computer simulations can start with the

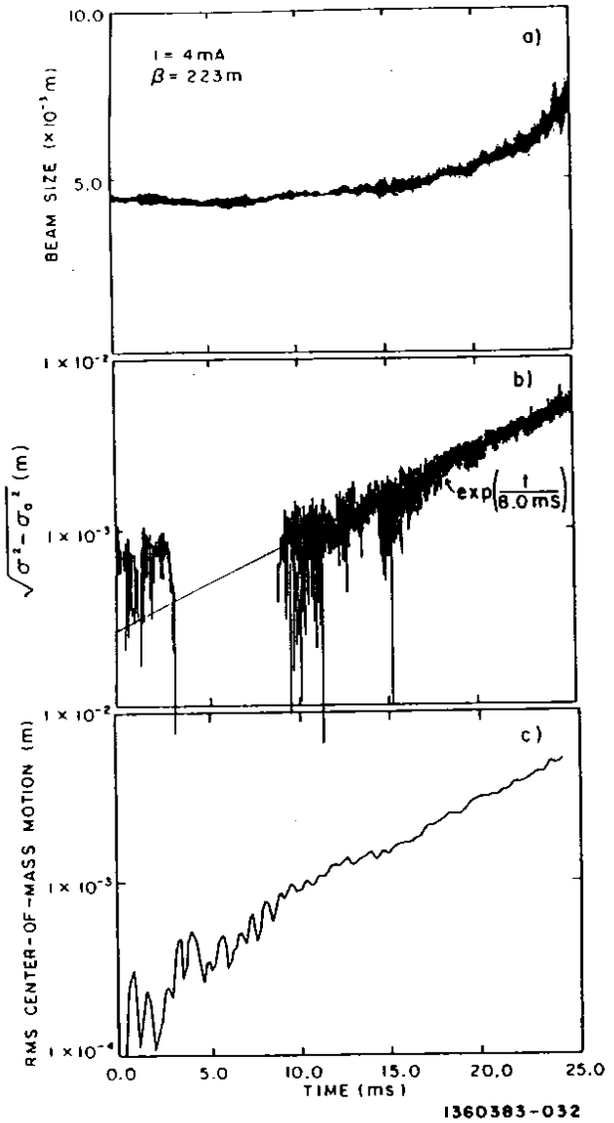

Fig. 19. The results of a computer simulation of beam stability in PEP. The current is just above threshold. The beam size ((a) and (b) where the natural size has been subtracted in (b)) and centroid motion (c) grow exponentially with an 8 ms time constant.[8]

geometry of components in the vacuum system, calculate wakefields from these geometries, and predict instability thresholds within a factor of two with NO free parameters! They have become important accelerator design tools.

The "Robinson Instability".[16] If beam induced fields last long enough, it is possible for energy and deflections to be transferred between bunches. This leads to multibunch and multiturn instabilities. A multiturn instability called the "Robinson instability" can result from the interaction of a beam with the fundamental (accelerating) mode of the RF cavity. It is modelled below with a single particle[15] and illustrates many aspects of multiple bunch instabilities.

When longitudinal wake potential of the RF cavity is included, eq. (3) becomes

$$\Delta\gamma \cong \frac{-eG\,L}{m\,c^2}\omega_{RF}\tau \quad + \frac{N\,e^2}{m\,c^2}\sum_n V_{\delta 0}(t_n) \quad \text{and} \quad \Delta\tau = 0. \tag{34}$$

The sum is over all previous turns. The equation of motion is that of a simple harmonic oscillator with a driving force from the wakefield

$$\frac{d^2\tau}{dt^2} + \omega_s^2\tau = \frac{N\,e^2}{\gamma_0 T_0 m\,c^2}\sum_n V_{\delta 0}(t_n) \ . \tag{35}$$

The wake potential has contributions from all the cavity resonant modes. The Robinson instability is due to the interaction with one of them, the fundamental, and this discussion concentrates on the fundamental mode. (Other modes lead to similar instabilities, and these are sometimes called Robinson instabilities also.) The fundamental mode has a quality factor Q and a natural frequency ω_n that is approximately equal to ω_{RF}. It is best to have $\omega_n \neq \omega_{RF}$ for the reasons that follow.

The wake potential due to the fundamental mode is shown in Figure 20a. Initially it is negative because of energy conservation (the same reason used when discussing Figure 13). It oscillates with frequency ω_n and decays as $\exp(-\omega_n t/2Q)$. The time elapsed between successive passages is $T_0 + \Delta\tau$ where $\Delta\tau$ is given by eq. (4). Only one term in the summation is kept for simplicity, and it can be approximated as

$$\begin{aligned} V_{\delta 0}(T_0+\Delta\tau) &\cong V_{\delta 0}(T_0) + \Delta\tau \left.\frac{dV_{\delta 0}}{dt}\right|_{T_0} + \ldots \\ &\cong V_{\delta 0}(T_0) + T_0 \frac{d\tau}{dt}\left.\frac{dV_{\delta 0}}{dt}\right|_{T_0} . \end{aligned} \tag{36}$$

Substituting eq. (36) into eq. (35) and ignoring the constant term because it doesn't have any effect on the dynamics gives

$$\frac{d^2\tau}{dt^2} - \left(\frac{N\,e^2}{\gamma_0 m\,c^2}\left.\frac{dV_{\delta 0}}{dt}\right|_{T_0}\right)\frac{d\tau}{dt} + \omega_s^2\tau = 0 \ . \tag{37}$$

If the overall coefficient of $d\tau/dt$ is positive, the motion is damped. However, if it is negative, τ grows exponentially. That is the Robinson instability. The criterion for stability can be restated as $dV_{\delta 0}/dt < 0$. Figure 20b shows the wakefield for three different values of ω_n. When $\omega_n = \omega_{RF}$, $\omega_n T_0$ is a multiple of 2π; the coefficient multiplying $d\tau/dt$ is zero and the cavity is "Robinson neutral". When $\omega_n > \omega_{RF}$, $dV_{\delta 0}/dt$ is positive, and the beam is unstable, but when $\omega_n < \omega_{RF}$, $dV_{\delta 0}/dt$ is negative, and there is no instability.

This conclusion is verified by more detailed calculations, and the Robinson instability is observed in storage rings when the RF cavities are improperly tuned. This and all other multibunch/multiturn instabilities are sensitive to the frequencies of resonant modes. When only the fundamental mode is of concern, the cavities can be tuned to avoid instability, but when additional resonant modes are important, it can be difficult to tune the cavities to

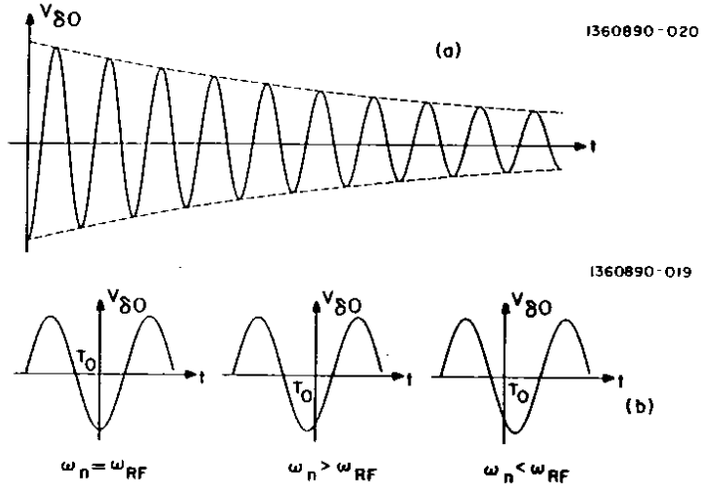

Fig. 20. The longitudinal wake potential for the fundamental mode. (a) shows the general behavior and (b) shows $V_{\delta 0}(t)$ near $t = T_0$ for three values of ω_n.

avoid these instabilities. Often quality factors must be lowered and/or feedback systems used to control multibunch instabilities.

Instability Categories. The physics of two instabilities has been illustrated above. There are other instabilities; these can be classified as:

1. Single bunch or multibunch/multiturn - the fast head-tail instability was single bunch and the Robinson instability was multiturn.
2. Transverse or longitudinal - the fast head-tail was transverse and Robinson instability longitudinal.
3. With or without centroid motion - this determines whether or not feedback can be used.
4. Self-limiting or having unbounded growth - longitudinal instabilities can be self-limiting because the equation of motion (eq. (2)) becomes nonlinear as τ gets large.

All possible combinations occur and have different importance depending on the particular accelerator. Most modern colliders are pushing one or more instability limits, and a general strategy is to reduce wakefields whenever possible by careful design of the vacuum chamber. Particular attention must be paid to minimizing the number and degree of discontinuities because, as Figure 11 shows, these are the sources of wakefields.

NONLINEAR FIELDS AND THEIR EFFECTS

The magnetic field of a quadrupole depends linearly on position (Figure 5), and a lattice of quadrupoles leads to betatron motion that is more complicated than simple harmonic motion but is linear - the oscillation frequency is independent of amplitude and the motion is stable for any amplitude. The size of the vacuum chamber determines the maximum amplitude. There are nonlinear fields in accelerators that arise from a number of sources. Some are intentional. For example, sextupoles are used to correct aberrations caused by quadrupoles. This is discussed in the next section about linear collider final focus systems. Other nonlinear fields are unavoidable consequences of methods that are used. Persistent currents that lead to nonlinear magnetic fields are such an unavoidable consequence of superconducting magnets, essential elements of high energy hadron colliders. Nonlinear fields often determine accelerator parameters and performance. This section discusses the causes and effects of these fields.

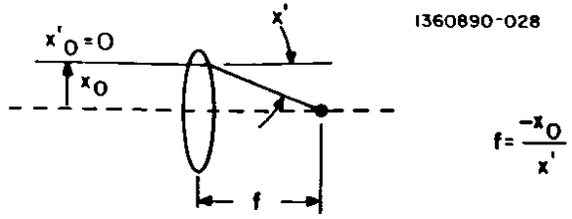

Fig. 21. The focal length of a thin lens.

Linear Collider Final Focus Systems

An ideal final focus system would have the same focusing properties independent of the energy of a particle, but a quadrupole focusing system has "chromatic aberrations" - energy dependent focusing properties. (A final focus system must focus in both transverse dimensions, and, therefore, must be a quadrupole triplet. This is ignored in the discussion that follows; only one transverse dimension and one quadrupole is analyzed.) Consider a focusing quadrupole of length L and gradient g. Equation (7) is the equation of motion. The position of a particle that enters the quadrupole with position and angle x_0 and x'_0, respectively, is

$$x = x_0 \cos(\kappa s) + x'_0 \sin(\kappa s) \qquad (38)$$

where s is the distance from the beginning of the quadrupole and

$$\kappa = \left(\frac{e|g|}{\gamma m c}\right)^{1/2}. \qquad (39)$$

By analogy with geometrical optics the focal length of the quadrupole can be found by looking at the trajectory with $x'_0 = 0$ (see Figure 21). That trajectory leaves the quadrupole with a slope

$$x' = -x_0 \kappa \sin(\kappa L) \cong -x_0 \kappa^2 L . \qquad (40)$$

It is assumed that the quadrupole is thin ($\kappa L << 1$) in the last step. The focal length,

$$f = \frac{1}{\kappa^2 L} = \frac{\gamma m c}{e|g|L}, \qquad (41)$$

gets longer, the lens gets weaker, as the energy increases. This is a chromatic aberration.

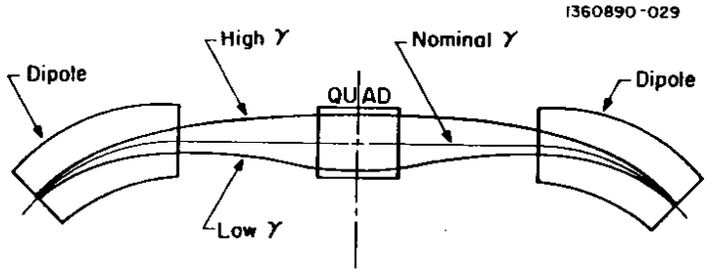

Fig. 22. A non-dispersive deflecting system.[17]

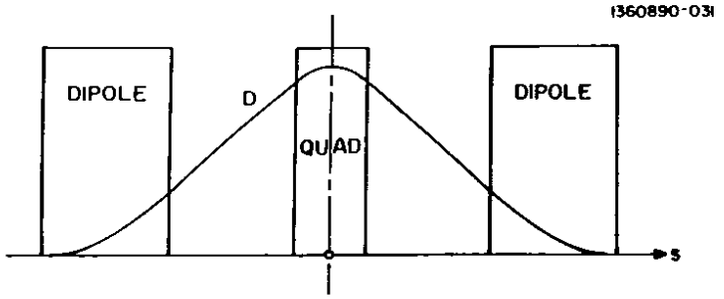

Fig. 23. The dispersion of the system in Figure 22.

This aberration can be corrected by a lens that gets stronger as the energy increases. That lens is a combination of dipoles, quadrupoles, and sextupoles. The dipoles and quadrupoles are arranged to form a "non-dispersive deflecting system".[17] A simple example is shown in Figure 22. A particle follows a path

$$x(s) = x_\beta(s) + D(s)\,\frac{\gamma-\gamma_0}{\gamma_0} \qquad (42)$$

where x_β is the betatron motion that depends on the initial position and angle and D(s) is the dispersion which is the trajectory of a particle with $x_0 = 0$, $x_0' = 0$, and energy γ. The first dipole produces dispersion. The quadrupole gives additional bending, and its strength is such that all trajectories with $x_0 = 0$ and $x_0' = 0$ are parallel at the symmetry point. The second dipole undoes the effect of the first one, and $D = 0$ at the exit of the system. The dispersion D(s) is plotted in Figure 23.

A sextupole, a magnet with $\phi = Sx^2y$ (Figure 24), placed in a region where $D \neq 0$ completes the construction of the desired lens. The magnetic field,

$$B_y = -Sx^2 = -S\left(x_\beta + D\,\frac{\gamma-\gamma_0}{\gamma_0}\right)^2 \qquad (43)$$

$$= -S\left(D\,\frac{\gamma-\gamma_0}{\gamma_0}\right)^2 - 2SD\left(\frac{\gamma-\gamma_0}{\gamma_0}\right)x_\beta - Sx_\beta^2 ,$$

has a quadrupole-like term (the second term) that increases with energy if S has the proper sign. The first term doesn't affect the betatron motion, so the price paid in constructing this

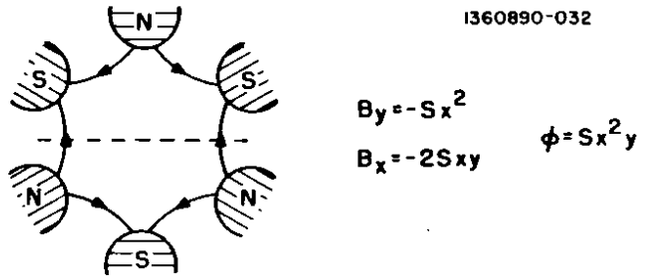

Fig. 24. A sextupole magnet.

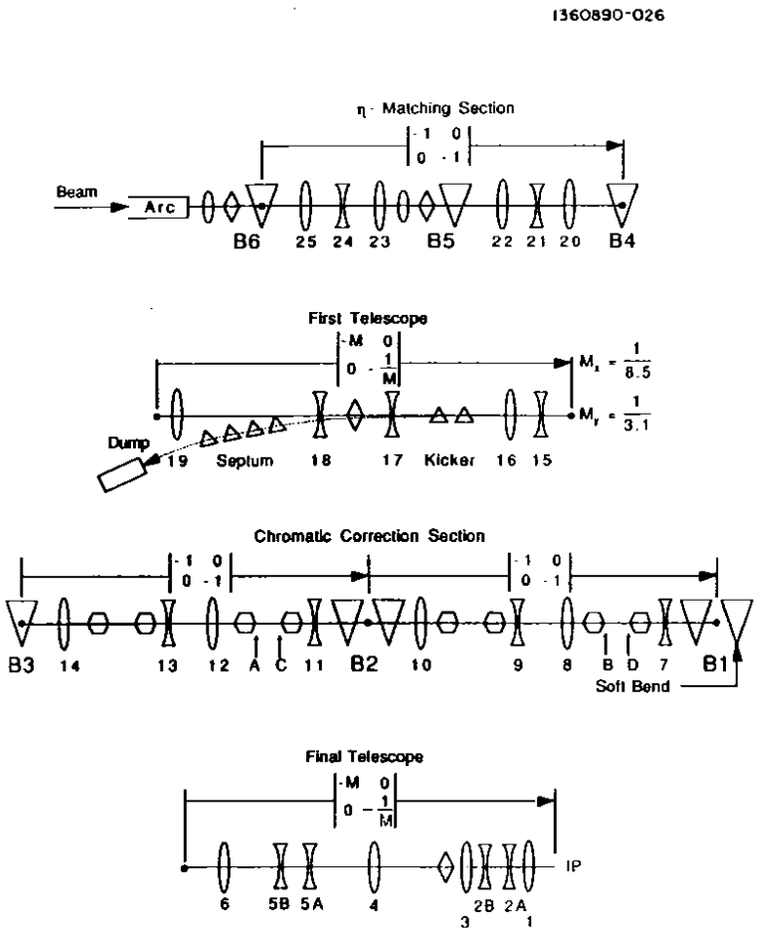

Fig. 25. The optical design of the SLC final focus system.[19] The discussion in the text is about a simplified "Chromatic Correction Section". Sextupoles are indicated by hexagons.

lens is the third term. The betatron equation of motion now has a nonlinear term! The chromatic aberration can be corrected by introducing a higher order "geometric aberration" - focusing that is not linear in the displacement.

This example points out: i) why nonlinear elements are used - with proper choice of magnet strengths a first order chromatic aberration can be eliminated, and ii) the problems they cause - a second order geometric aberration was introduced. The example was simplified because only one dimension was considered. Two dimensions and real B fields lead to more complicated systems. In addition, the example doesn't show how clever placement of the magnets can eliminate some of the geometric aberrations.[18] The design and construction of a final focus system with good optical properties is an art; Figure 25 illustrates this.[19]

Nonlinear Effects in Storage Rings

Chromaticity. Quadrupoles confine the beams in storage rings, and, therefore, the focusing, β-functions, phase advances, and tunes are momentum dependent. The chromaticity, defined as

$$\xi = \frac{\gamma}{Q_\beta}\frac{dQ_\beta}{d\gamma} \quad . \tag{44}$$

is negative, $\xi \sim -1$, because the quadrupoles get weaker as the energy increases. There are several reasons to want $\xi \geq 0$. First, the tune spread caused by chromaticity should be small to allow a tune spread from the beam-beam interaction. This is discussed in the section on beam-beam effects. Second, avoiding the "head-tail" instability (related to but different from the fast head-tail instability) requires $\xi > 0$.[20]

The orbit length in a storage ring is energy dependent (eq. (4)), and, therefore, the orbit itself must be energy dependent. This energy dependence is described by off-energy functions, called η-functions, which are solutions to the same equations as the dispersion, D, but with the boundary condition that η is periodic, $\eta(s + C) = \eta(s)$. The displacement of a particle with energy γ is given by eq. (42) with $\eta(s)$ replacing D(s). The η-functions in the SSC interaction region are shown in Figure 10. In the arcs $\eta_y = 0$ and η_x has a smooth, periodic behavior similar to the β-functions. Sextupoles installed in the arcs are used to correct the chromaticity just as they are used to correct chromatic aberrations in final focus systems. Figure 26 shows a section of CESR as an example. The price for using sextupoles is the introduction of nonlinear fields and geometric aberrations that lead to an effective aperture - the "dynamic aperture".

A Single Octupole. The dynamic aperture is the dominant accelerator physics issue in the SSC, LHC, and synchrotron light rings. The chromaticity correcting sextupoles are strong in the latter, and they determine the dynamic aperture. The dominant nonlinear fields in high energy hadron colliders are due to persistent currents in superconducting magnets and not intentional sextupoles. Put aside the causes of nonlinear fields in this section and concentrate on their effects.

The easiest problem to analyze is a single octupole in a storage ring (Figure 27).[21] The octupole is treated as a perturbation of the betatron motion, and an octupole is chosen because all of the important effects show up in the first order perturbation expansion. The expansion must be done to second order to see all of the effects of a sextupole. The octupole is treated as a thin element, so in passing through half of it the position and angle change as

$$\Delta x = 0, \quad \Delta x' = B_3 x^3 \quad . \tag{45}$$

A particle entering the arc with initial coordinate x_0 and angle x_0' leaves with

$$x = x_0 \cos(2\pi Q_0) + \beta x_0' \sin(2\pi Q_0)$$
$$x' = -\frac{x_0}{\beta}\sin(2\pi Q_0) + x_0' \cos(2\pi Q_0) \quad . \tag{46}$$

Fig. 26. The Wilson Laboratory tunnel. The 10-GeV synchrotron is on the left and CESR on the right. The small CESR magnet in the foreground is a chromaticity correcting sextupole. It is followed by a quadrupole and dipoles. Prof. B. D. McDaniel, director of the laboratory at the time of CESR construction, is in the background.

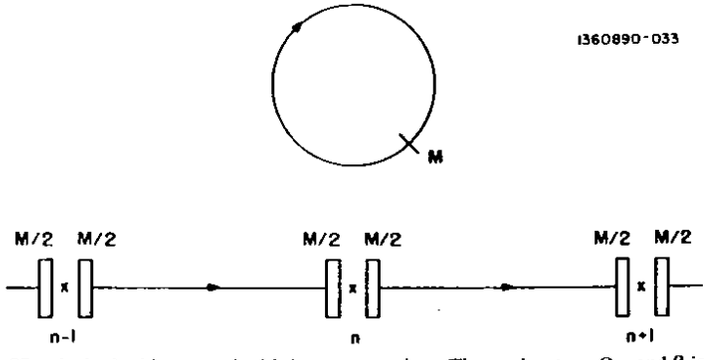

Fig. 27. A single thin octupole, M, in a storage ring. The arc has tune Q_0, and β is the value of the β-function at M. Turn numbers are defined in the middle of M.

The position on turn n, x_n, is

$$x_n = x_{n-1}\cos(2\pi Q_0) + (x'_{n-1} + B_3 x^3_{n-1})\beta \sin(2\pi Q_0) \quad . \tag{47}$$

Similar expressions can be written for $x'_n + \Delta x'_n$ and x_{n+1}, and these can be combined with eq. (47) to give a nonlinear equation

$$x_{n+1} - 2\cos(2\pi Q)x_n + x_{n-1} = 2\beta \sin(2\pi Q_0) B_3 x^3_n + 2x_n[\cos(2\pi Q_0) - \cos(2\pi Q)] \tag{48}$$

where Q is the actual tune that differs from Q_0 because of the octupole.

Solve this equation by Fourier analysis and perturbation. Write x_n as a Fourier series

$$x_n = \sum_{r=1}^{\infty} a_r \cos(2\pi r Q n) \tag{49}$$

where $a_1 >> a_2, a_3, \ldots$. Writing the right-hand-side (RHS) of eq. (48) as a Fourier series also,

$$\text{RHS} = \sum_{r=1}^{\infty} c_r \cos(2\pi r Q n), \tag{50}$$

gives a relationship between the Fourier coefficients

$$a_r = \frac{c_r}{2[\cos(2\pi r Q) - \cos(2\pi Q)]} \quad . \tag{51}$$

The first step in the perturbation treatment is to substitute the leading term in eq. (49), $x_n \cong a_1\cos(2\pi Q n)$ into the right-hand-side of eq. (48). Then

$$\begin{aligned} c_1 &= 2a_1\left(\cos(2\pi Q_0) - \cos(2\pi Q) + \tfrac{3}{4}\beta B_3 a_1^2 \sin(2\pi Q_0)\right), \\ c_3 &= \tfrac{1}{2}\beta B_3 a_1^3 \sin(2\pi Q_0), \\ c_r &= 0 \quad \text{if} \quad r \neq 1, 3. \end{aligned} \tag{52}$$

Equation (51) has many of the features of nonlinear motion. First, the tune Q is a function of amplitude

$$\cos(2\pi Q) = \cos(2\pi Q_0) + \tfrac{3}{4}\beta B_3 a_1^2 \sin(2\pi Q_0) \tag{53}$$

because a_1 would be infinite unless $c_1 = 0$. There is no tune shift with amplitude for a sextupole if analyzed with the same first order perturbation treatment, but it does appear in second order and is proportional to the square of the sextupole strength. Second, there are resonances caused by the nonlinearity which have infinite response in this order of perturbation. In the octupole example $c_3 \neq 0$, and $a_3 = \infty$ when $\cos(6\pi Q) = \cos(2\pi Q)$, i.e. when $4Q = m$ where m is any integer. The response won't be infinite in a more complete analysis, but it is enhanced at these particular tunes. The particular values of Q are consequences of having chosen an octupole. Other multipoles have different resonant tunes; for a sextupole they are $3Q = m$.

The problem of a single octupole can be simulated also. Figure 28 shows the results. Particles are started at an initial amplitude A_0 and are followed for 1000 turns. When A_0 is small, the amplitude at the end of 1000 turns (calculated using eq. (20)) is approximately equal to A_0, $A_{1000} \sim A_0$. The initial amplitude is increased until a value is reached where $A_{1000} > 10\ A_0$. That value of A_0 is called the maximum initial amplitude and is plotted versus Q_0 in Figure 28. The amplitude of a particle that has reached $10\ A_0$ in 1000 turns is increasing rapidly, and the results are not sensitive to the definition of the maximum amplitude or the number of turns.

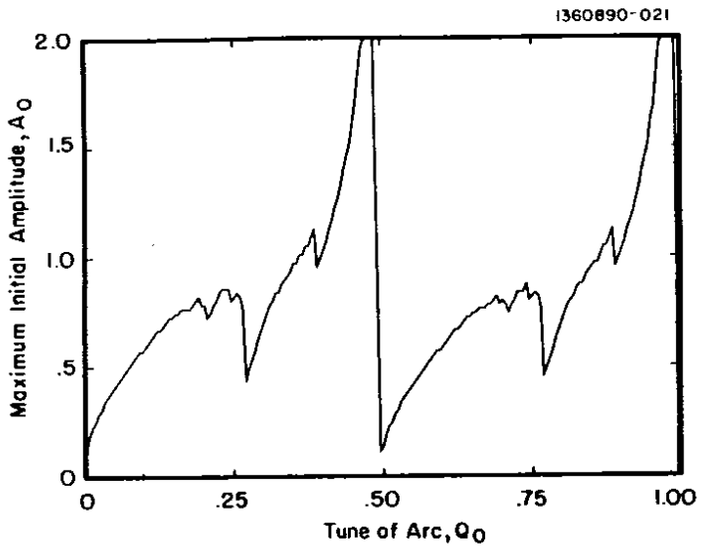

Fig. 28. The results of a computer simulation of a single thin octupole, M, in a storage ring. The maximum initial amplitude is plotted versus the tune of the arc, Q_0. This example used $\beta = 1$ m and $B_3 = 0.5$ T/m^3.

The most striking feature of these results is that there are such maximum amplitudes. A particle starting at A_0(max) is unstable. Its amplitude grows rapidly, and it will hit the vacuum chamber wall no matter how far away. Figure 28 is a plot of the dynamic aperture of a linear storage ring with a single octupole! The dynamic aperture is tune dependent. There is an overall trend with some fine structure due to resonances. The $4Q = m$ resonances predicted by the first order perturbation expansion are seen clearly. They are much stronger when m is an even integer. When m is odd the resonances are weaker, and they seem to be displaced from the expected value; however, that is not the case because the resonant conditions depend on Q and not Q_0. Resonances are seen at $Q_0 \sim 3/8$, 7/8 also. These are higher order resonances, and they would appear in a higher order perturbation expansion.

This single octupole example has shown the important consequences of of nonlinear fields. They lead to tunes that depend on amplitude, resonances at particular tunes, and a dynamic aperture. Equations (51) and (52) show that effects depend on the strength of the nonlinear field and the β-function at the location of the nonlinearity.

The Dynamic Aperture in High Energy Hadron Colliders. Superconducting magnets are current dominated; the **B** field is determined by the location of the current carrying conductors and not the location of the surrounding iron. A current density

$$J_z(\theta, r) = I\ \delta(r - r_c)\cos\theta \tag{54}$$

produces a dipole field (Figure 29). The conductors in a real dipole are arranged in an approximation of a cos θ distribution as illustrated in Figure 30. Nonlinear fields can arise from errors in conductor placement and persistent currents.[21a] Persistent currents are currents that are induced in type II superconductors as the superconductor attempts to exclude flux (the Meisner effect). They flow in single filaments of superconductor. Each filament forms a magnetic dipole, $\mu = I_p D$, where D is the diameter of the filament and the persistent current I_p depends on many factors including the critical current density (which

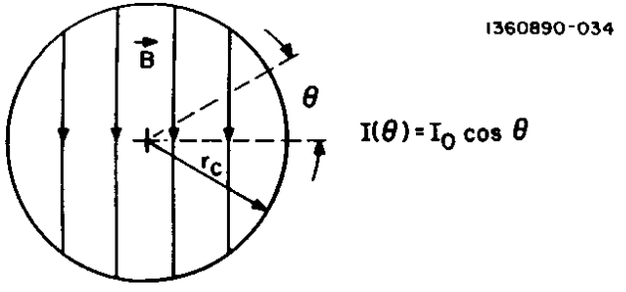

Fig. 29. An idealized superconducting dipole.

in turn depends on the local magnetic field and the operating temperature), the amount of transport current in the superconductor, the previous magnetic history of the superconductor, and time. The time dependence was unexpected and was discovered at the Tevatron;[22] the cause is still uncertain. The magnet multipoles due to conductor placement errors depend on the coil radius, r_c, as $B_n \sim 1/r_c^{n+1}$ where n = 1 is the quadrupole moment, n = 2 the sextupole moment, etc. The multipoles due to persistent currents vary as $B_n \sim I_p D/r_c^{n+2}$.

High energy hadron colliders, the SSC and LHC, will have a limited dynamic aperture due to the nonlinear fields in the dipoles. The aperture at the injection energy is the most critical because i) the persistent currents are large there, ii) the beam energy is low and the beam is less rigid, and iii) the beam is large - the size is proportional to $1/\sqrt{\gamma}$ because the emittance falls as $1/\gamma$. Having an adequate dynamic aperture is a clear and obvious design requirement, but going from that requirement to accelerator specifications requires a great deal of judgement for the following reasons:

1. Phenomena occur on different time scales ranging from the decay time constants of the persistent currents to the injection and storage times.
2. Corrections are possible. The beam itself can be used as a diagnostic to understand and improve the dynamic aperture. How much should one rely on this?
3. The specifications are sensitive to assumptions made about the parameters of subsystems and components. Superconductor properties, operating temperature spread, and even the power supply regulation are important.
4. The physics of the dynamic aperture is nonlinear dynamics, and that is an active field of research with articles appearing each month in Physical Review Letters.

Despite all these uncertainties the accelerator designers must make choices, and that is where the judgement enters.

The discussion above is sufficient to understand the considerations that go into the choices. First, the superconducting filament size should be minimized. Research into the properties, metallurgy, and manufacturing of superconducting wires has been successful in increasing the critical current and reducing the filament size. This research was motivated in part by the SSC, and these advances are incorporated into the SSC and LHC designs. Second, raising the injection energy increases the effective dynamic aperture for the reasons enumerated above. Third, all of the nonlinear multipoles decrease as strong powers of the coil radius. For example, the persistent current sextupole varies as r_c^{-4}, and this sextupole moment can be reduced by a factor of two with less than 25% increase in r_c. Fourth, the sensitivity to nonlinear multipoles can be reduced by reducing the β-function. This was shown in the section on the single octupole. All of these ways of increasing the dynamic aperture were used in the recent changes of the SSC design.

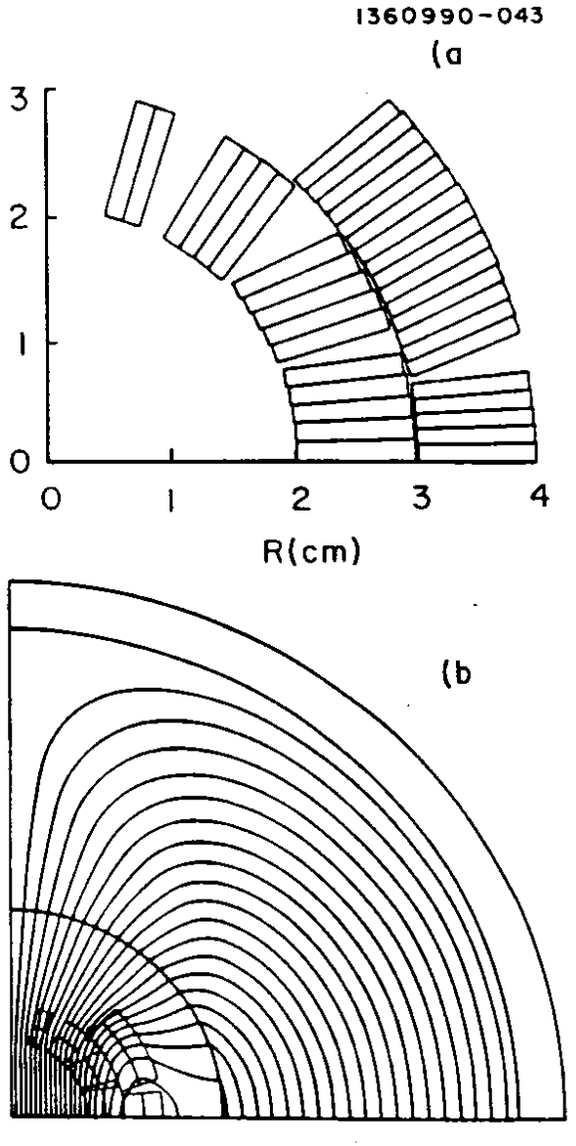

Fig. 30. A quadrant of a dipole cross section showing a) the distribution of superconducting cable and b) the magnetic field lines.[23]

Table 1. Storage Ring - Linear Collider Comparison

STORAGE RINGS	*LINEAR COLLIDERS*
The collision area is large, and high luminosity is made possible by a high collision frequency.	The collision frequency is small, and high luminosity is made possible by a small effective area.
The beams are reused.	The beams are used once.
Single collisions are "gentle", and the physics of the beam-beam interaction is that of nonlinear fields and nonlinear resonances.	Single collisions are violent, and the physics of the beam-beam interaction is plasma physics and quantum electrodynamics.
There is a wealth of experimental experience, and the understanding is guided by this experience.	There is limited experimental experience.

THE BEAM-BEAM INTERACTION

The center-of-mass energy, the types of beams, and the luminosity are the accelerator properties of primary importance to experimenters. For them

$$\text{Rate}(\text{sec}^{-1}) = L(\text{cm}^{-2}\text{sec}^{-1}) \times \sigma(\text{cm}^2) \qquad (55)$$

where σ is the cross section of interest. The accelerator physicist thinks about the luminosity in terms of beam parameters

$$L = \frac{N^2 f_c}{4\pi\sigma_x\sigma_y} \qquad (17')$$

where N is the number of particles per bunch, f_c is the collision frequency and $4\pi\sigma_x\sigma_y$ is the effective collision area for Gaussian beams. The hard collisions that produce elementary particles are relatively rare, and the dominant interaction is between the particles of one beam and the electromagnetic fields of the other. This is the beam-beam interaction.

The beam-beam interaction is dramatically different in linear colliders and storage rings. They are compared in Table 1.

The Electromagnetic Fields

Begin by considering the electromagnetic fields of a flat, uniform charge distribution of width W, height H, and length D (Figure 31). The electric field at $x = 0$ and $y < H/2$ is

$$E_y = \frac{1}{\epsilon_0}\frac{N e}{WD}\frac{y}{H} \qquad (56)$$

where ϵ_0 is the permittivity of free space. There is a magnetic field also. If the beams are relativistic, it is $B_x = E_y/c$ (see the coordinate system in Figure 31). The effects of the electric and magnetic fields add, and

$$\frac{dp_y}{dt} = -\frac{2}{\epsilon_0}\frac{N e^2}{WD}\frac{y}{H} \qquad (57)$$

where the minus sign comes from assuming oppositely charged beams. This equation of motion is that of a particle in a focusing quadrupole. When the collisions are gentle as in a storage ring this uniform charge distribution is a lens with focal length

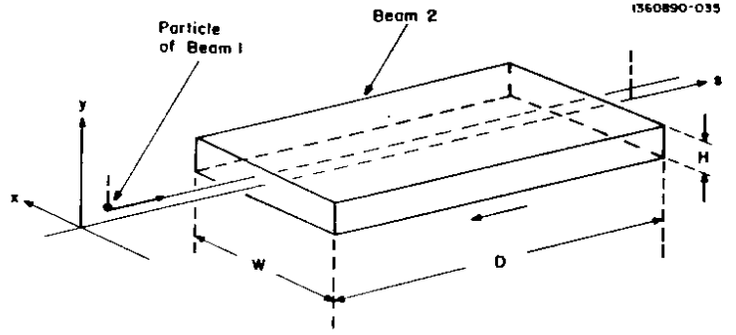

Fig. 31. A flat, uniform charge distribution. W >> H is assumed in the discussion.

$$f = \frac{\gamma W H}{8\pi r_e N} ; \qquad (58)$$

$r_e = e^2/4\pi\epsilon_0 mc^2$ is the classical electron radius.

The close connection between the luminosity and the beam-beam interaction can be seen by comparing eqs. (17') and (56). Both are proportional to the number of particles divided by the effective area ($4\pi\sigma_x\sigma_y$ for the Gaussian beam assumed in eq. (17') and WH for the uniform beams used for eq. (56)). Limitations on the beam generated fields have consequences for the luminosity.

Beams are not uniform. Gaussian distributions are a much better approximation. The electromagnetic fields for a Gaussian distribution are linear near the center of the beam where the equations of motion are[24]

$$\frac{d^2 z}{ds^2} = \frac{1}{\gamma m c^2}\frac{dp_z}{dt} = -\frac{2N r_e}{\gamma}\frac{1}{\sigma_x+\sigma_y}\frac{z}{\sigma_z}S(s) \qquad (59)$$

where z = x or y and S(s) is longitudinal density distribution. The quantities $N/[\gamma(\sigma_x+\sigma_y)\sigma_x]$ and $N/[\gamma(\sigma_x+\sigma_y)\sigma_y]$ set the scale of the beam-beam interaction near the center of the beam. The disruption parameters in linear colliders and the beam-beam tune spreads in storage rings are proportional to them. The fields fall as $1/(x^2+y^2)^{1/2}$ when x, $y >> \sigma_x, \sigma_y$, and in the intermediate region they make the transition between the central and large distance behaviors. This is illustrated in Figure 32. The nonlinearity of the fields at $y \sim \sigma_y$ is important for the beam-beam interaction in storage rings.

Beam-Beam Effects in Linear Colliders

A particle can be focused by the fields of the opposing beam - this is called "disruption", and it can radiate and produce pairs in those fields - the radiation is called "beamstrahlung". Figure 33 shows all of this. Consider disruption first.

Disruption. When the fields are weak, particles in the center of the beam are focused by a lens with focal lengths $f_{x,y} = \sigma_s/D_{x,y}$ where σ_s is the bunch length in meters and $D_{x,y}$ are the "disruption parameters" given by

$$D_z = \frac{2 r_e N \sigma_s}{\gamma(\sigma_x+\sigma_y)\sigma_z} \quad (z = x \text{ or } y) . \qquad (60)$$

This follows from eq. (59). As the disruption increases the focal length decreases, and when $f \sim \sigma_s$ the beam-beam interaction cannot be described in the terms of geometrical

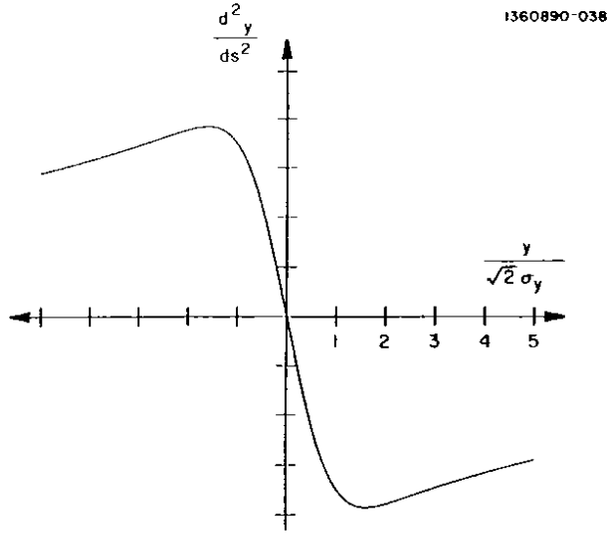

Fig. 32. d^2y/ds^2 near x = 0 for a flat beam ($\sigma_x >> \sigma_y$).

optics. Particles in both beams are strongly focused, and the charge distributions evolve during the collision. This problem has to be studied with computer simulations. The result is that particles undergo a number of plasma oscillations given by $n \cong (D/10.4)^{1/2}$.[25] Figure 34 shows the evolution of the distribution of one of the beams during a collision with moderate disruption.

The luminosity is enhanced by disruption - the focusing reduces the effective collision area. Simulations have been used to estimate the enhancement factor.[25,26] These simulations make different assumptions and approximations and use different numerical methods. The results are sensitive to the differences (Figure 35). Some experimental results would clarify the situation, but it is unlikely that this will happen soon - in 1991 ~10% enhancement is expected at the SLC.[27] Future linear colliders are being designed with flat rather than round beams. The reasons are associated with beamstrahlung and pair production and are discussed below. The luminosity enhancement is not as great with flat beams; for $D_y \sim 5$ (and $D_x << D_y$) the enhancement factor is about two.

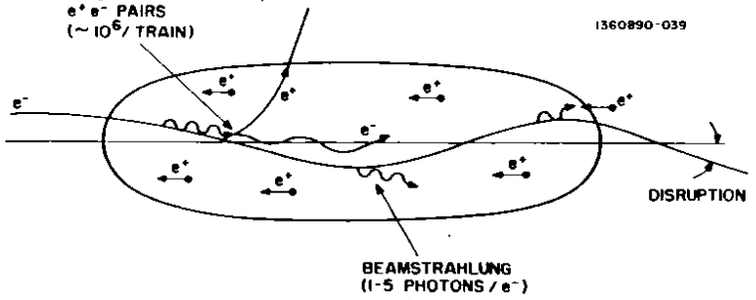

Fig. 33. The processes in the beam-beam interaction in linear colliders.

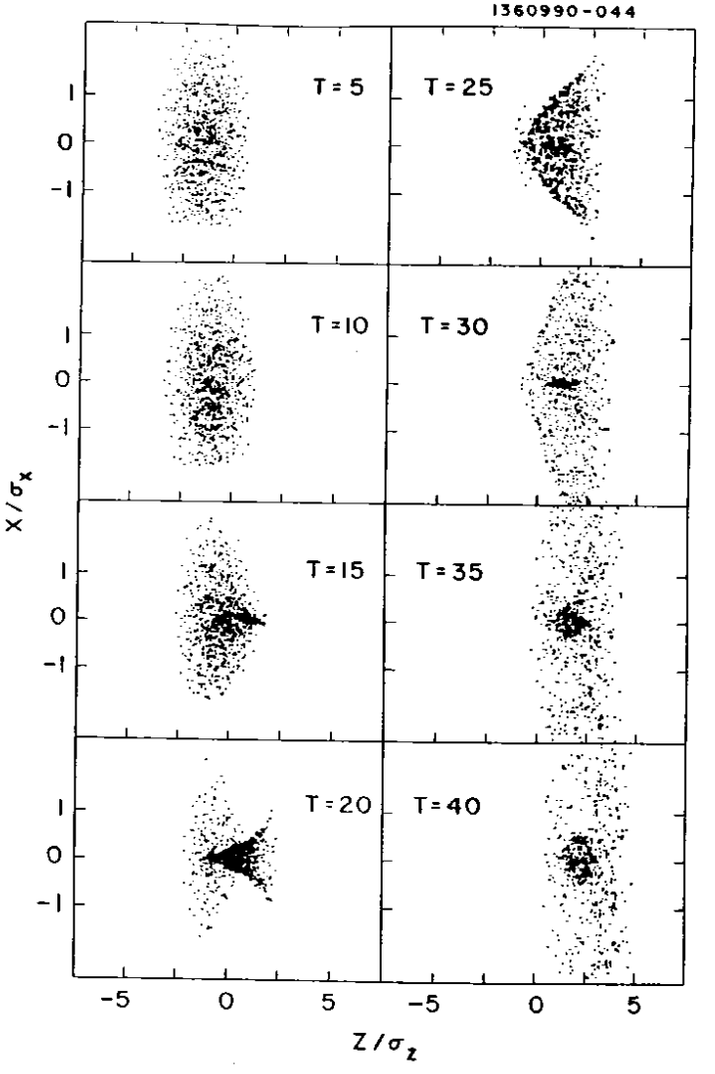

Fig. 34. The transverse density distributions during the collision of two round Gaussian beams with D = 3. The locations of test particles in the beam moving to the right are plotted as time advances during the collision. The particles in the beam moving to the left are not plotted.[25]

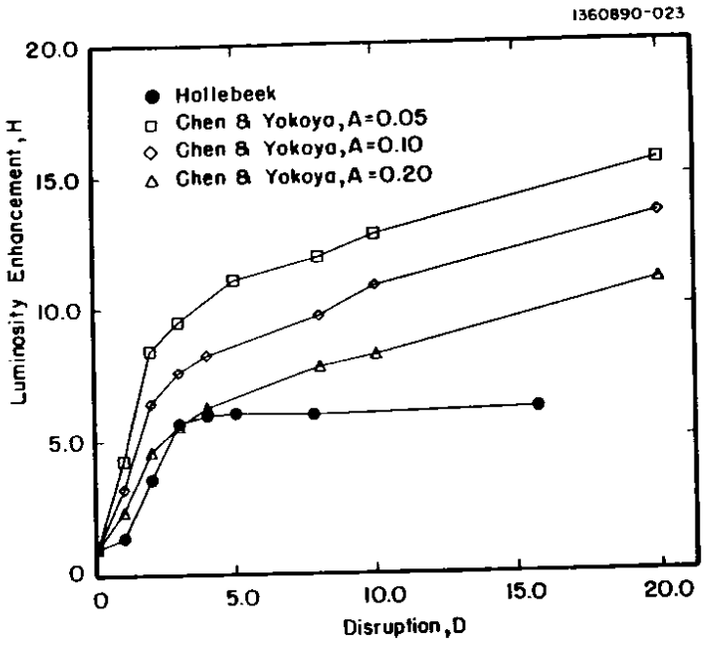

Fig. 35. Luminosity enhancement due to disruption from Hollebeek[25] and Chen and Yokoya.[26] These results are for round beams, and the parameter A is defined by Chen and Yokoya as $A = \varepsilon\gamma D/r_e N$. A = 0 in the Hollebeek calculation.

A consequence of disruption is that the beams have large angular divergences when they leave the interaction point. Simulation results for flat beams can be fit by[28]

$$\theta_y(\mathrm{rms}) \sim \frac{0.55}{[1+(D_y/2)^5]^{1/6}} \frac{D_y\sigma_y}{\sigma_s} , \qquad (61)$$

and $\theta_y(\mathrm{max}) \sim 2.5\,\theta_y(\mathrm{rms})$. These angles are a fraction of a milliradian for typical parameters. The beam transport must be designed to accommodate the disrupted beams as they leave the interaction point to avoid backgrounds. The present thinking is to have the beam collide at a small angle and to have large aperture exit paths in the final focus quadrupoles. If that is done the disrupted beams probably will not be the critical source of backgrounds.

Beamstrahlung. The electromagnetic fields at the interaction point are so large that beamstrahlung (radiation) and pair production dominate linear collider designs. The beamstrahlung spectrum is characterized by a scaling parameter[29]

$$\Upsilon \sim \frac{r_e^2\gamma N}{\alpha(\sigma_x+\sigma_y)\sigma_s} \qquad (62)$$

where $\alpha = 1/137$ is the fine structure constant. When $\Upsilon \ll 1$ the beamstrahlung spectrum is a classical synchrotron radiation spectrum that peaks at an energy $E \sim E_c/3$ where E_c is called the critical energy. It is related to Υ by $\Upsilon = 2/3\times(E_c/E_{beam})$. A collider with $\Upsilon \ll 1$ is said to operate in the "classical" beamstrahlung regime. The SLC and most likely the next linear collider are in the classical regime. When $\Upsilon \gg 1$ the spectrum must be calculated quantum mechanically,[30] and the collider is in the "quantum" beamstrahlung regime.

A second parameter characterizing beamstrahlung, δ, is the average fractional energy loss of a particle during the collision. The dependences of δ on beam sizes, N and γ are different in the classical and quantum regimes[12]

$$\delta_{cl} = 0.88\frac{r_e^3N^2\gamma}{\sigma_s(\sigma_x+\sigma_y)^2} , \quad \delta_q = 0.56\frac{\delta_{cl}}{\Upsilon^{4/3}} \quad (\Upsilon \gtrsim 10) . \qquad (63)$$

The fractional energy loss is important for experimenters because it determines the average value of and the spread in the center-of-mass energy. Expressions for the luminosity, δ, and the beam power ($P_b = \gamma mc^2 N f_c$) can be combined to give scaling relationships for linear colliders[12]

$$\frac{L^2\gamma^3}{\delta_{cl}} = 7.2\times10^{-3}\frac{(\sigma_x+\sigma_y)^2\sigma_s H P_b^2}{r_e^3(mc^2)^2\sigma_x^2\sigma_y^2} , \qquad (64)$$

and

$$\frac{L^2\gamma}{\delta_q^3} = 5.0\times10^{-2}\frac{(\sigma_x+\sigma_y)^2 H P_b^2}{\alpha^4 r_e(mc^2)^2\sigma_x^2\sigma_y^2\sigma_s} \qquad (65)$$

(H is the luminosity enhancement from disruption). The quantities on the left-hand-sides are determined by particle physics, and they give a relationship between the beam sizes and the beam power. The latter is the dominant contribution to the operating cost because the beam power must come from the AC mains with some efficiency for converting mains power to beam power.

Equations (64) and (65) show the constraints that beam-beam effects put on collider parameters. In particular, they show that the luminosity can be enhanced for a given δ with a flat beam, and this is one of the reasons that linear collider designers are concentrating on flat beams. The underlying reason comes from eqs. (17') and (56). They show that the typical electromagnetic field of the beam scales as

$$E_y(\mathrm{typ.}) \propto \left(L\frac{H}{W}\right)^{1/2} , \qquad (66)$$

and this field determines the deflection of a particle and the amount it radiates.

Pair Production. It was realized about two years ago that there would be copious pair production in the beam-beam interaction in linear colliders. There are two processes. One is incoherent pair production - beamstrahlung photons interact with individual particles in the oncoming beam to produce pairs, for example $\gamma e^- \rightarrow e^+e^-e^-$. The cross section is large, and $\sim 10^6$ pairs are produced per beam burst.[28] The second process is coherent pair production where beamstrahlung photons interact with the fields of the bunch rather than with an individual particle. The relative importance is determined by the scaling parameter Υ defined in eq. (62).[28] When $\Upsilon \ll 1$ (the classical beamstrahlung regime) coherent pair production is not important. When $\Upsilon \gg 1$ (the quantum regime) it is the dominant process, and the number of pairs per burst can be 10^7 or more.[28]

Linear colliders must be designed to minimize the impact of this potential background. Flat beams help by keeping Υ small and thereby avoiding coherent pair production. Equation (66) has the underlying reason again; the fields are reduced for a flat beam. The second way to control this background is having the beams collide at an angle. One particle in the pair is focused by the oncoming beam (see Figure 33) and exits along the axis with the disrupted beam. The other particle in the pair is expelled from the collision region by the high fields of the oncoming beam, but it is captured in a spiral trajectory by the solenoidal field of the detector. Therefore, both particles in the pair travel in the forward

direction. A crossing angle separates the paths of the incoming and exiting beams and allows a large aperture exit for the disrupted beam and the shielding appropriate for dumping the large halo of pairs. A disadvantage of colliding at an angle is that the effective overlap area is increased and luminosity is lost, but this can be solved by tilting the beams with an RF deflector just before the interaction region.[31] This "crab crossing" idea appears again in the discussion about beam-beam effects in storage rings.

Beam-Beam Effects in Storage Rings

This is a problem in nonlinear dynamics. The force is not a linear function of the displacement (Figure 32), and this leads to amplitude dependent tunes, resonances, and the possibility of a dynamic aperture. The dynamics of the beam-beam interaction differs from that produced by nonlinear magnetic fields in several ways:

1. There are many resonances in the first order perturbation expansion. The single octupole problem had resonances at $4Q = m$, but the simplest beam-beam problem - a round beam, a linear transport, and a single interaction point - has resonances at $2nQ = m$ where m and n are integers.
2. The beam-beam fields fall-off rather than increase at large displacements. Large amplitude particles experience a small beam-beam force, and their motion is almost linear. There isn't a dynamic aperture except near resonant tunes.
3. The force depends on the beam distribution, and that can evolve in time. This opens up additional possibilities including collective beam-beam effects similar to the instabilities driven by wakefields.

Begin by estimating the amplitude dependent tunes. The electromagnetic fields are linear with displacement for small distances from the center of the beam (eq. (59)). They act like a focusing quadrupole and have all of the effects of such a quadrupole on the betatron motion. Particles with small oscillation amplitudes (eq. (14)) have betatron tunes, Q_x and Q_y, that are greater than the values they would have with no beam-beam interaction, $Q_z \cong Q_{z0} + \xi_z$ where

$$\xi_z = \frac{r_e}{2\pi} \frac{N \beta_z^*}{\gamma(\sigma_x+\sigma_y)\sigma_z} \quad (z = x \text{ or } y). \tag{67}$$

Equation (67) follows from the expressions for the fields (eq. (59)) and the effects of a quadrupole error (eq. (16)). Large amplitude particles experience a small beam-beam force that is not quadrupole-like. Therefore, their motion is almost linear, and they have tunes $Q_z \cong Q_{z0}$. The parameters ξ_x and ξ_y are the spreads in tunes. They are often called the "beam-beam tune shifts" because they are the tune shifts of the small amplitude particles. This name is misleading; it implies that the problem is a linear problem and it isn't - all particles do not have the same tune shifts. It is better to call the ξ's the "beam-beam tune spreads".

The tune spreads characterize the strength of the beam-beam interaction. The empirical limit in hadron colliders is based on experience in the Spp̄S and Tevatron; it is[32]

$$N_{ip} \xi \leq 0.024 \tag{68}$$

where N_{ip} is the number of interaction points and ξ ($\xi_x \cong \xi_y$) is the tune spread from one interaction point. There is a simple explanation for this limit.[33] The beam-beam interaction and nonlinear magnets produce resonances. If the discussion of a single octupole was extended to two dimensions and other nonlinearities, it would be found that the resonance condition is $mQ_x + nQ_y = p$ (m, n & p are integers). There are infinitely many such resonances, but their strength gets weaker as the resonance order, |m| + |n|, gets higher. Particles that fall on any low order resonances - have tunes that satisfy the resonance condition for a low order resonance - are lost from the storage ring. Low order resonances must be avoided, and eq. (68) is a measure of the amount of tune spread that can be accommodated without particles falling on low order resonances.

The situation is more complicated in e^+e^- storage rings. There are data from many more colliders, but these data do not show consistent patterns or trends.[34] A great deal of attention has been focused on the effects of synchrotron radiation because it was thought that it would reduce further the strength of high order resonances and allow a larger tune spread than in hadron colliders. The data indicate that there are other, more important effects. A rough summary of the data is that in different e^+e^- colliders the maximum tune spreads (both ξ_x and ξ_y) are in the range

$$0.01 \leq \xi \text{ (max)} \leq 0.07 . \tag{69}$$

Large tune spreads are important! Suppose that the number of particles per bunch or the total number of particles were limited by instabilities, the number of $\bar{p}$'s one can make, etc. Then

$$L = \xi_y \frac{\gamma N f_c (1+\sigma_y/\sigma_x)}{2 r_e \beta_y^*} \tag{70}$$

where $\xi_x = \xi_y$ has been assumed for simplicity. The tune spread measures the efficiency for using the particles to make luminosity. If there are no limits on the number of particles $L \propto \xi^2$, and a large tune spread is even more valuable.

There are a number of related questions. What limits the tune spreads? How can the tune spreads be increased? How can the data from the e^+e^- colliders be understood better? In my opinion the answers to all these questions are related to the nonlinearity of the beam-beam interaction and the nature of the resulting resonances. When the synchrotron oscillations are included along with the two transverse dimensions, the resonance condition becomes $mQ_x + nQ_y + pQ_s = r$ (m, n, p & r are integers and Q_s is the synchrotron tune), and the resonance order is |m| + |n| + |p|. Synchrotron motion is not important for hadron colliders because Q_s is low and resonances involving the synchrotron motion would be high order. However, it is important for e^+e^- colliders because the synchrotron tune can be large ($Q_s \sim 0.05$ is not unusual), and low order resonances involving synchrotron motion are possible.

The years of experience with e^+e^- storage rings have led to some empirical rules for getting large tune spreads. Most of these rules are ways to avoid resonances. Table 2 gives the rules, brief statements about the physics, and the original references. Understanding the

Table 2. Beam-Beam Rules and Ideas

RULE	*Ref.*	*EXPLANATION*
$\beta_x^*, \beta_y^* > \sigma_s$	37	The betatron phase advance on successive turns is modulated by synchrotron oscillations. Recent work suggests that this rule may not be as stringent as once thought.[38,39]
$\eta^* = 0$	37	η^* is the η-function at the interaction point. If $\eta^* \neq 0$, the horizontal position is energy dependent; this modulates the beam-beam deflection at Q_s.
Head-on collisions	35	With non-zero crossing angle the beam-beam deflection is modulated by synchrotron oscillations.
IDEA	*Ref.*	*EXPLANATION*
Round beams	40	The modulation of the vertical deflection by horizontal betatron oscillations is removed.[41]
Crab crossing	36	Tilting the beam removes the modulation introduced by non-zero crossing angle.

Fig. 36. Two bunches colliding at an angle. Particles 1, 2 & 3 are part of the unshaded bunch. a) through e) show the passage of time during the collision, and f) shows the positions of the particles in longitudinal phase space. 1360890-037

Fig. 37. A collision one-quarter of a synchrotron oscillation period later.

Fig. 38 A collision with crab crossing.

physics of these empirical rules leads to ideas about new modes of operation that could have higher tune spreads. Two such ideas are included in Table 2. Crab crossing and head-on collisions are related closely, and they are discussed as an example.

Figure 36 shows two bunches colliding at an angle. Particle #1 at the head of its bunch passes through the head of the oncoming bunch while particle #2 passes through the center and particle #3 passes through the tail. Particle #2 is deflected more than #1 and #3 because the charge density of the opposing bunch is greater at the center than at the head or tail. One-quarter of a synchrotron oscillation period later the situation is different (Figure 37). Particles #1 and #3 are in the center of the bunch, and #2 is at the tail. Therefore, #1 and #3 experience larger deflections than #2. The beam-beam deflection is modulated by synchrotron oscillations, and this leads to synchrobetatron resonances - resonances involving Q_s. The collisions must be head-on to avoid this modulation. The beams in DORIS I crossed at an angle, and DORIS I had a low maximum tune spread.[35] That experience led to the rule that collisions must be head-on.

Colliding at an angle could be attractive for high luminosity because a high collision frequency would be possible. Crab crossing which was discussed above can be adapted to storage rings to permit crossing at an angle.[36] It is illustrated in Figure 38. The bunches cross at an angle, but they are tilted with respect to their directions of propagation. Each of the three particles pass through the head, center, and tail of the opposing bunch, and they have the same beam-beam deflection. The source of the modulation with synchrotron motion and the resonance are removed while still having a crossing angle. The cost is that RF cavities with deflecting fields are needed at each side of the interaction point to tilt the bunches before and remove the tilt after the collision.

Considerations such as those above are central to the design of heavy quark factories and the planned upgrades of the Tevatron collider because these accelerators are pushing other limits on N or $N \times f_c$. Efficient utilization of the current is essential for high luminosity.

CONCLUDING REMARK

Accelerators are key instruments for particle physics. They are interesting physical systems in their own right also. I hope these lecture notes show that and give experimenters some appreciation for the work of their colleagues in the accelerator part of our science.

REFERENCES

1. Edwin M. McMillan, Phys. Rev. 68, 143(1945).
2. E. Courant and H. Snyder, Annals of Physics **3**, 27 (1958).
3. Site-Specific Conceptual Design for the SSC, ed. D. Matthews (1990).
4. Herbert Goldstein, Classical Mechanics, Addison-Wesley Publishing Company, Reading, Mass. (1959).
5. An excellent reference for electron storage rings is M. Sands, The Physics of Electron Storage Rings - An Introduction, SLAC-121 (SLAC, 1970).
6. T. Weiland, CERN/ISR-TH/80-07 (CERN, 1980).
7. R. H. Siemann, Proc. of the 17th SLAC Summer Institute, ed. E. C. Brennan, p. 263 (1990).
8. R. H. Siemann, AIP Conf. Proc. **127**, 368 (1985).
9. W. K. H. Panofsky and W. A. Wentzel, Rev. Sci. Inst. **27**, 967 (1956).
10. K. L. F. Bane, IEEE Trans. Nucl. Sci. **NS-32**, 3565 (1985).
11. V. E. Balakin, A. V. Novokhatsky, and V. P. Smirnov, Proc. of 12th Int. Conf. on High Energy Accel., ed. F. Cole, R. Donaldson, p. 119 (1983).
12. P. B. Wilson, SLAC-PUB-3674, (SLAC, 1985).
13. W. Schnell, CERN-LEP-RF/87-24, (CERN, 1987).
14. R. D. Kohaupt, Proc. of the 11th Int. Conf. on High Energy Accel., ed W. S. Newman, p. 562 (1980).
15. This analysis comes from A. Chao, AIP Conf. Proc. **105**, 353 (1983).
16. K. Robinson, CEAL Report TM-183 (CEA, 1969).
17. Klaus G. Steffen, High Energy Beam Optics, Interscience Publishers, New York (1965).
18. K. L. Brown and R. V. Servranckx, AIP Conf. Proc. **127**, 62 (1985).
19. R. A. Erickson, AIP Conf. Proc. **184**, 1554 (1989).
20. C. Pellegrini, Nuovo Cimento **LXIV**, 447 (1969).
21. This analysis is from R. Talman, AIP Conf. Proc. **153**, 835 (1987).

21a. H. E. Fisk et al, Proc. of the 1984 Summer Study on the Design and Utilization of the SSC, edited by R. Donalson and J. G. Morfin, p. 329 (1984).

22. R. P. Johnson, Proc. of the 1987 IEEE Accel. Conf., ed. E. R. Lindstrom and L. S. Taylor, p. 8 (1987).
23. SSC Conceptual Design, ed. J. D. Jackson (1986).
24. M. Bassetti and G. Erskine, CERN-ISR-TH/80-06, (CERN, 1980).
25. R. Hollebeek, Nucl. Inst. & Methods **184**, 333 (1981).
26. P. Chen and K. Yokoya, Phys. Rev. **D38**, 987 (1988).
27. M. Breidenbach et al, SLC Performance in 1991, (SLAC, 1990).
28. P. Chen, AIP Conf. Proc. **184**, 633 (1989).
29. T. Himel and J. Siegrist, AIP Conf. Proc. **130**, 602 (1985).
30. R. Blankenbecler and S. D. Drell, Phys. Rev. **D36**, 277 (1987).
31. R. Palmer, SLAC-PUB-4707 (SLAC, 1989).
32. R. Schmidt and M. Harrison, to be published in Proc. of 1990 European Part. Accel. Conf..
33. L. Evans, AIP Conf. Proc. **127**, 243 (1985).
34. J. Seeman, Nonlinear Dynamics Aspects of Particle Accelerators, Springer-Verlag, Berlin, edited by J. M. Jowett, S. Turner and M. Month, p. 121 (1986).
35. A. Piwinski, IEEE Trans. Nucl. Sci. **NS-24**, 1408 (1977).
36. K. Oide and K. Yokoya, Phys. Rev. **A40**, 315 (1989).
37. F. M. Izrailev and I. B. Vasserman, 7th All Union Conf. on Charged Part. Accel., p. 288 (1981).
38. D. Rice, Part. Accel. **31**, 1315 (1990).
39. S. Krishnagopal and R. Siemann, Phys. Rev. **D41**, 2312 (1990).
40. S. Krishnagopal and R. Siemann, Proc. of the 1989 IEEE Part. Accel. Conf., edited by F. Bennett and J. Kopta, p. 836 (1989).
41. S. Peggs and R. Talman, Phys. Rev. **D24**, 2379 (1983).